ATLAS PUB Note
ATL-PHYS-PUB-2023-039
28th November 2023

Standard Model Summary Plots October 2023

The ATLAS Collaboration

This note presents cross-section summary plots for ATLAS cross-section measurements as of October 2023. Figures with references contain hyperlinks to ATLAS publications and preliminary documentation.

Contents

1 Introduction

This document summarizes the Standard Model summary plots with the inputs available at 04/10/2023. The scripts for the creation of these plots are available at [1].

2 Updates since March 2022

Since the last publication of these summary plots [2], the following results have been updated:

- **Total and inelastic pp** cross-section at 13 TeV: The total and inelastic cross-section measurements are published as a paper using an integrated luminosity of 340 μb^{-1} [3].
- $t\bar{t}t\bar{t}$ at 13 TeV: More precise results are available with full Run 2 dataset [4].
- **s-channel single top** at 13 TeV: The cross-section measurements are done with full Run 2 dataset [5].
- $H \rightarrow b\bar{b}$ at 13 TeV: The fiducial cross-section is measured with Run 2 dataset, using an integrated luminosity of 126 fb^{-1} [6].
- **t-channel single top** at 5 and 13 TeV : The inclusive production cross-section has been measured using 255 pb^{-1} [7] at 5 TeV. The cross-section are now available with full Run 2 dataset at 13TeV [8].
- $t\bar{t}$ at 5 TeV and 13 TeV: More precise results are available at 5 TeV [9] and with full Run 2 dataset at 13 TeV [10].
- $t\bar{t}W$ at 13 TeV: The inclusive production cross-section has been measured with full Run 2 dataset [11].

- $t\bar{t}Z$ at 13 TeV: The inclusive production cross-section has been measured with full Run 2 dataset [12].
- $Z\gamma\gamma$ at 13 TeV: The production cross-section is measured with full Run 2 dataset [13].
- $W\gamma\gamma$ at 13 TeV: The inclusive fiducial production cross-section is measured with full Run 2 dataset [14].
- $WZ\gamma$ at 13 TeV: The cross-section measurements is available with full Run 2 dataset [15].
- $W^{\pm}W^{\pm}jj$ at 13 TeV: The measured electroweak production cross-section is now available with full Run 2 dataset [16].
- **Z** at 13.6 TeV: The cross-section is measured with Run 3 dataset, using an integrated luminosity of 1.29 fb^{-1} [17].
- **ZZ** at 13.6 TeV: The cross-section is available with Run 3 dataset, using an integrated luminosity of 29 fb^{-1} [18].
- H at 13.6 TeV: The measured total Higgs, $H \to \gamma\gamma$ and $H \to ZZ$ production cross-sections are available with Run 3 dataset, using an integrated luminosity of 31.4 and 29 fb^{-1} [19].
- $t\bar{t}/Z$ at 13.6 TeV: The inclusive top-quark-pair production cross section and its ratio to the Z-boson production cross section have been measured with Run 3 dataset, using an integrated luminosity of 29 fb^{-1} [20].

  Also, tables are rearranged to better represent values used for measured cross-sections and associated predictions for the results shown in all figures.

Only Figures 1, 2, 3, 5, 6, 8, 9, 11, 15, 16, 17, 18, 19, 20, 26 and 27 are affected by the aforementioned updates.

3 Total cross section overview plots

Figures 1 and 2 summarize several Standard Model total production cross-section measurements, corrected for branching fractions, compared to the corresponding theoretical expectations. The luminosity used for each measurement is indicated in the table. Some measurements have been extrapolated using branching ratios as predicted by the Standard Model for the Higgs boson. Uncertainties for the theoretical predictions are quoted from the original ATLAS papers. They were not always evaluated using the same prescriptions for PDFs and scales.

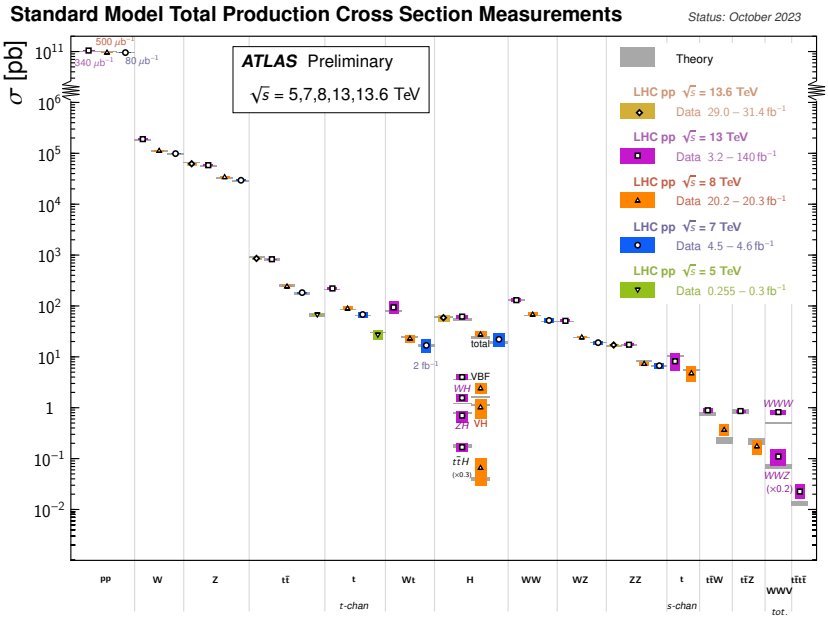

(a)

Standard Model Production Cross Section Measurements

Status: October 2023

ATLAS Preliminary
$\sqrt{s}$ = 5, 7, 8, 13, 13.6 TeV

Model	E_{CM} [TeV]	$\int \mathcal{L}\,dt$[fb^{-1}]	Measurement	Theory	Reference
pp	13	34×10^{-8}	$\sigma = 104.7 \pm 0.22 \pm 1.07$ mb	$\sigma = 100.3 \pm 0.12$ mb (COMPETE HPR1R2)	EPJC 83 (2023) 441
pp	8	50×10^{-8}	$\sigma = 96.07 \pm 0.18 \pm 0.91$ mb	$\sigma = 99.55 \pm 2.14$ mb (COMPETE HPR1R2)	PLB 761 (2016) 158
pp	7	8×10^{-8}	$\sigma = 95.35 \pm 0.38 \pm 1.3$ mb	$\sigma = 97.26 \pm 2.12$ mb (COMPETE HPR1R2)	Nucl. Phys. B (2014) 486
W	13	0.081	$\sigma = 190.1 \pm 0.2 \pm 6.4$ nb	$\sigma = 184.9 + 6 - 6.1$ nb (DYNNLO + CT14NNLO)	PLB 759 (2016) 601
W	8	20.2	$\sigma = 112.69 \pm 3.1$ nb	$\sigma = 110.919889503 \pm 3.7$ nb (DYNNLO + CT14NNLO)	EPJC 79 (2019) 760
W	7	4.6	$\sigma = 98.71 \pm 0.028 \pm 2.191$ nb	$\sigma = 95.9 \pm 2.9$ nb (DYNNLO + CT14NNLO)	EPJC 77 (2017) 367
Z	13.6	1.2	$\sigma = 61.65 \pm 0.059 \pm 2.91$ nb	$\sigma = 64.83 + 1.25 - 1.34$ nb (NNLO(QCD)+NLO(EW))	ATLAS-CONF-2022-070
Z	13	3.2	$\sigma = 58.43 \pm 0.03 \pm 1.66$ nb	$\sigma = 55.96 + 1.5 - 1.7$ nb (DYNNLO+CT14 NNLO)	JHEP 02 (2017) 117
Z	8	20.2	$\sigma = 34.24 \pm 0.03 \pm 0.92$ nb	$\sigma = 32.94 + 0.8 - 0.92$ nb (DYNNLO+CT14 NNLO)	JHEP 02 (2017) 117
Z	7	4.6	$\sigma = 29.53 \pm 0.03 \pm 0.77$ nb	$\sigma = 28.31 + 0.68 - 0.8$ nb (DYNNLO+CT14 NNLO)	JHEP 02 (2017) 117
tt̄	13.6	29.0	$\sigma = 850 \pm 3 \pm 27$ pb	$\sigma = 924 + 32 - 40$ pb (top++ NNLO+NNLL)	arXiv:2308.09529
tt̄	13	140	$\sigma = 829 \pm 1 \pm 15.4$ pb	$\sigma = 832 + 46.4 - 50.9$ pb (top++ NNLO+NNLL)	JHEP 07 (2023) 141
tt̄	8	20.2	$\sigma = 242.9 \pm 1.7 \pm 8.6$ pb	$\sigma = 252.9 + 13.3 - 14.5$ pb (top++ NNLO+NNLL)	EPJC 74 (2014) 3109
tt̄	7	4.6	$\sigma = 182.9 \pm 3.1 \pm 6.4$ pb	$\sigma = 177 + 10 - 11$ pb (top++ NNLO+NNLL)	EPJC 74 (2014) 3109
tt̄	5	0.3	$\sigma = 67.5 \pm 0.9 \pm 2.6$ pb	$\sigma = 68.2 + 5.2 - 5.3$ pb (top++ NNLO+NNLL)	JHEP 06 (2023) 138
t_{t-chan}	13	140	$\sigma = 221 \pm 1 \pm 13$ pb	$\sigma = 214.2 + 4.1 - 2.6$ pb (MCFM (NNLO))	ATLAS-CONF-2023-026
t_{t-chan}	8	20.3	$\sigma = 89.6 \pm 1.7 + 7.2 - 6.4$ pb	$\sigma = 84.3 + 1.7 - 1.2$ pb (MCFM (NNLO))	EPJC 77 (2017) 531
t_{t-chan}	7	4.6	$\sigma = 68 \pm 2 \pm 8$ pb	$\sigma = 63.7 + 1.4 - 0.8$ pb (MCFM (NNLO))	PRD 90, 112006 (2014)
t_{t-chan}	5	0.3	$\sigma = 27.1 - 4.4 - 4.1 + 4.4 - 3.7$ pb	$\sigma = 30.3 + 0.7 - 0.5$ pb (MCFM (NNLO))	arXiv:2310.01518
Wt	13	3.2	$\sigma = 94 \pm 10 + 28 - 23$ pb	$\sigma = 79.3 + 2.9 - 2.8$ pb (NLO+NNLL)	JHEP 01 (2018) 63
Wt	8	20.3	$\sigma = 23 \pm 1.3 + 3.4 - 3.7$ pb	$\sigma = 24.4 + 1.1 - 1$ pb (NLO+NLL)	JHEP 01, 064 (2016)
Wt	7	2.0	$\sigma = 16.8 \pm 2.9 \pm 3.9$ pb	$\sigma = 17.1 \pm 0.8$ pb (NLO+NLL)	PLB 716, 142-159 (2012)
H	13.6	31.4	$\sigma = 58.2 \pm 7.5 \pm 4.5$ pb	$\sigma = 59.9 \pm 2.6$ pb (LHC-HXSWG YR4)	arXiv:2306.11379
H	13	139	$\sigma = 55.5 \pm 3.2 + 2.4 - 2.2$ pb	$\sigma = 55.6 \pm 2.5$ pb (LHC-HXSWG YR4)	JHEP 05 (2023) 028
H	8	20.3	$\sigma = 27.7 \pm 3 + 2.3 - 1.9$ pb	$\sigma = 24.5 + 1.3 - 1.8$ pb (LHC-HXSWG YR4)	EPJC 76 (2016) 6
H	7	4.5	$\sigma = 22.1 + 6.7 - 5.3 + 3.3 - 2.7$ pb	$\sigma = 19.2 + 1 - 1.4$ pb (LHC-HXSWG YR4)	EPJC 76 (2016) 6
H VBF, $\lvert y_H\rvert < 2.5$	13	139	$\sigma = 4 \pm 0.3 + 0.3 - 0.4$ pb	$\sigma = 3.51 \pm 0.07$ pb (LHC-HXSWG)	Nature 607, pages 52-59 (2022)
H VBF	8	20.3	$\sigma = 2.43 + 0.5 - 0.49 + 0.33 - 0.26$ pb	$\sigma = 1.6 \pm 0.04$ pb (LHC-HXSWG YR4)	EPJC 76 (2016) 6
VH	8	20.3	$\sigma = 1.03 + 0.37 - 0.36 + 0.26 - 0.21$ pb	$\sigma = 1.12 \pm 0.03$ pb (NNLO(QCD)+NLO(EW))	JHEP 12 (2017) 024
WH, $\lvert y_H\rvert < 2.5$	13	139	$\sigma = 1.56 + 0.2 - 0.21 + 0.16 - 0.18$ pb	$\sigma = 1.203 \pm 0.024$ pb (Powheg Box NLO(QCD))	Nature 607, pages 52-59 (2022)
ZH, $\lvert y_H\rvert < 2.5$	13	139	$\sigma = 0.7 \pm 0.13 + 0.1 - 0.12$ pb	$\sigma = 0.795 \pm 0.03$ pb (Powheg Box NLO(QCD))	Nature 607, pages 52-59 (2022)
tt̄H	13	139	$\sigma = 560 \pm 80 + 70 - 80$ fb	$\sigma = 580 \pm 50$ fb (LHCHXSWG NLO QCD + NLO EW)	Nature 607, pages 52-59 (2022)
tt̄H	8	20.3	$\sigma = 220 \pm 100 \pm 70$ fb	$\sigma = 133 + 8 - 13$ fb (LHCHXSWG NLO QCD + NLO EW)	PLB 784 (2018) 173
WW	13	36.1	$\sigma = 130.04 \pm 1.7 \pm 10.6$ pb	$\sigma = 128.4 + 3.2 - 2.9$ pb (NNLO)	EPJC 79 (2019) 884
WW	8	20.3	$\sigma = 68.2 \pm 1.2 + 4.6$ pb	$\sigma = 65 + 1.2 - 1.1$ pb (NNLO)	PLB 763, 114 (2016)
WW	7	4.6	$\sigma = 51.9 \pm 2 \pm 4.4$ pb	$\sigma = 49.04 + 1.03 - 0.88$ pb (NNLO)	PRD 87 (2013) 112001, PRL 113 (2014) 212001
WZ	13	36.1	$\sigma = 51 \pm 0.8 \pm 2.3$ pb	$\sigma = 49.1 + 1.1 - 1$ pb (MATRIX (NNLO))	EPJC 79 (2019) 535
WZ	8	20.3	$\sigma = 24.3 \pm 0.6 \pm 0.9$ pb	$\sigma = 23.92 \pm 0.4$ pb (MATRIX (NNLO))	PRD 93, 092004 (2016)
WZ	7	4.6	$\sigma = 19 + 1.4 - 1.3 \pm 1$ pb	$\sigma = 19.34 + 0.3 - 0.4$ pb (MATRIX (NNLO))	EPJC 72 (2012) 2173
ZZ	13.6	29.0	$\sigma = 16.9 \pm 0.7 \pm 0.7$ pb	$\sigma = 16.7 \pm 0.4$ pb (Matrix (NNLO) & Sherpa (NLO))	ATLAS-CONF-2023-062
ZZ	13	36.1	$\sigma = 17.3 \pm 0.6 \pm 0.8$ pb	$\sigma = 16.9 + 0.6 - 0.5$ pb (Matrix (NNLO) & Sherpa (NLO))	PRD 97 (2018) 032005
ZZ	8	20.3	$\sigma = 7.3 \pm 0.4 + 0.4 - 0.3$ pb	$\sigma = 8.284 + 0.249 - 0.191$ pb (NNLO)	JHEP 01, 099 (2017)
ZZ	7	4.6	$\sigma = 6.7 \pm 0.7 + 0.5 - 0.4$ pb	$\sigma = 6.735 + 0.195 - 0.155$ pb (NNLO)	JHEP 03, 128 (2013), PLB 735 (2014) 311
t_{s-chan}	13	140	$\sigma = 8.2 \pm 0.6 + 3.4 - 2.8$ pb	$\sigma = 10.32 + 0.4 - 0.36$ pb (NLO+NNLL)	JHEP 06 (2023) 191
t_{s-chan}	8	20.3	$\sigma = 4.8 \pm 0.8 + 1.6 - 1.3$ pb	$\sigma = 5.61 \pm 0.22$ pb (NLO+NNLL)	PLB 756 (2016) 228-246
tt̄W	13	140	$\sigma = 890 \pm 50 \pm 70$ fb	$\sigma = 745 \pm 52$ fb (NNLOQCD + NLOEW)	ATLAS-CONF-2023-019
tt̄W	8	20.3	$\sigma = 369 + 86 - 79 \pm 44$ fb	$\sigma = 232 \pm 32$ fb (MCFM)	JHEP 11, 172 (2015)
tt̄Z	13	140	$\sigma = 860 \pm 40 \pm 40$ fb	$\sigma = 860 + 80 - 90$ fb (NLO + NNLL)	ATLAS-CONF-2023-065
tt̄Z	8	20.3	$\sigma = 176 + 52 - 48 \pm 24$ fb	$\sigma = 215 \pm 30$ fb (HELAC-NLO)	JHEP 11, 172 (2015)
WWW	13	139	$\sigma = 0.82 \pm 0.01 \pm 0.08$ pb	$\sigma = 0.511 \pm 0.018$ pb (NLO QCD)	PRL 129 (2022) 061803
WWZ	13	79.8	$\sigma = 0.55 \pm 0.14 - 0.15 - 0.13$ pb	$\sigma = 0.358 \pm 0.036$ pb (Sherpa 2.2.2)	PLB 798 (2019) 134913
tt̄tt̄	13	140	$\sigma = 22.5 + 4.7 - 3.4 + 6.6 - 5.5$ fb	$\sigma = 13.4 + 1 - 1.8$ fb (NLO QCD + EW)	EPJC 83 (2023) 496

(b)

Figure 1: Summary of several Standard Model cross-section measurements (a) with associated references (b). The measurements are corrected for branching fractions, compared to the corresponding theoretical expectations.

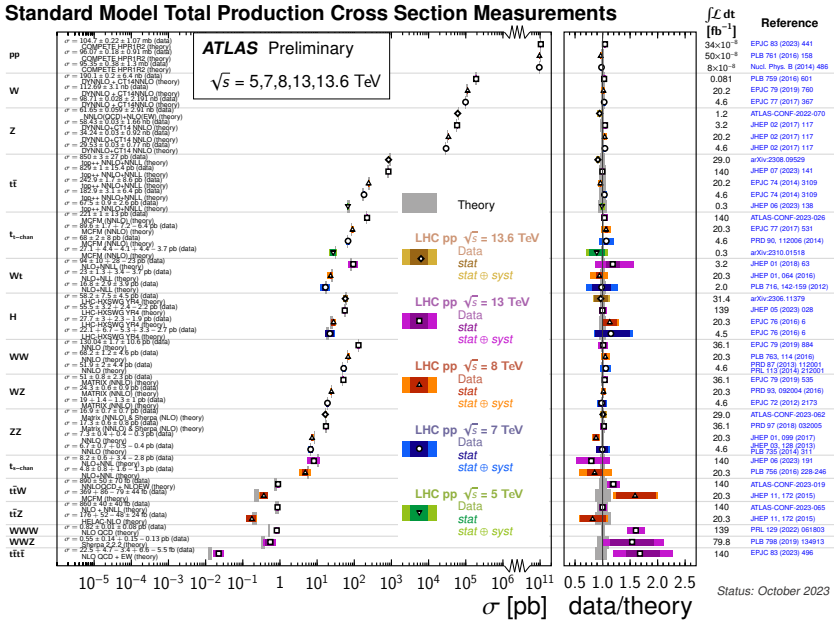

Figure 2: Summary of several Standard Model total production cross-section measurements, corrected for branching fractions, compared to the corresponding theoretical expectations and ratio with respect to theory. The associated references can also be found in Table 1(b).

4 Fiducial cross section overview plots

Figures 3, 4, 5, 6, 7, 8, 9, 10 and 11 summarize several Standard Model total and fiducial production cross-section measurements. Where total cross sections are reported, the measurements are corrected for branching fractions and compared to the corresponding theoretical expectations. For the measurement of the tZj production process at 13 TeV, the fiducial volume definition was updated to require $m_{\ell\ell} > 30\,\text{GeV}$. Some measurements have been extrapolated using branching ratios as predicted by the Standard Model for the Higgs boson. Uncertainties for the theoretical predictions are quoted from the original ATLAS papers. They were not always evaluated using the same prescriptions for PDFs and scales.

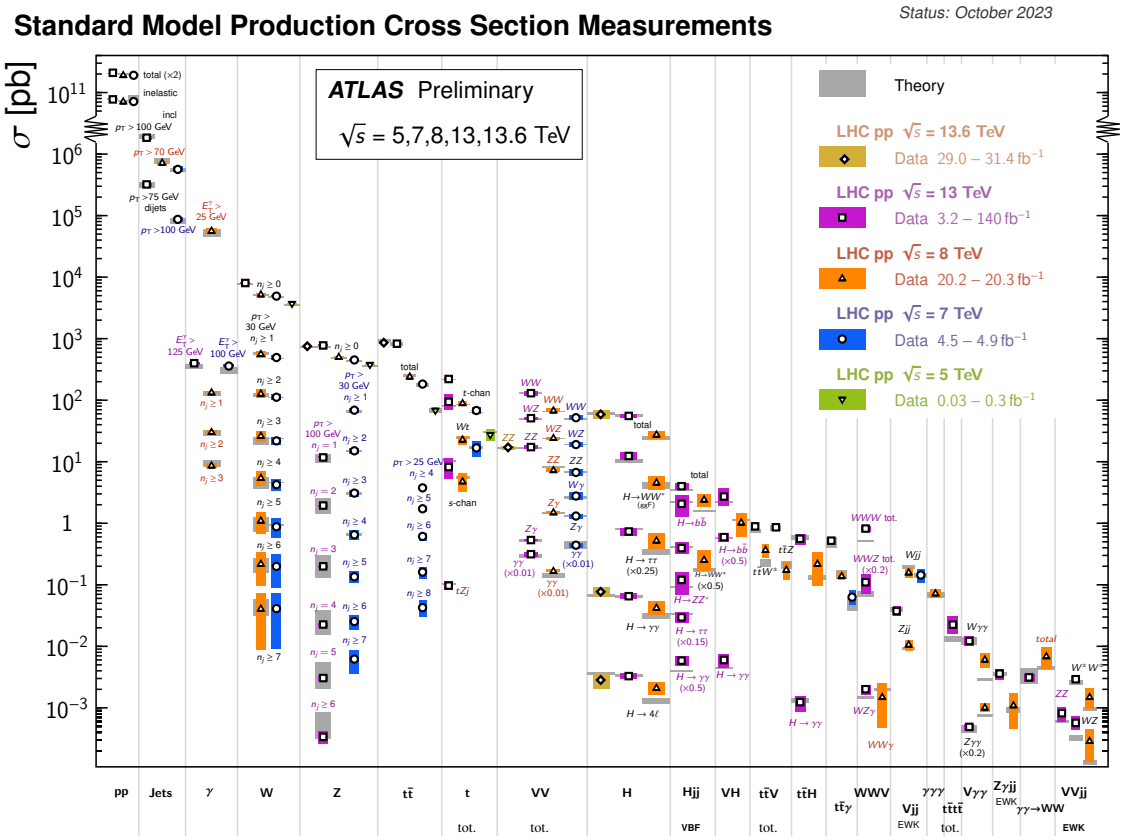

(a)

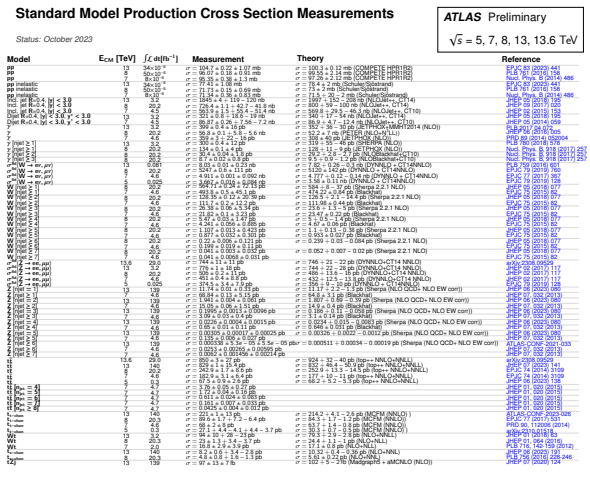

(b)

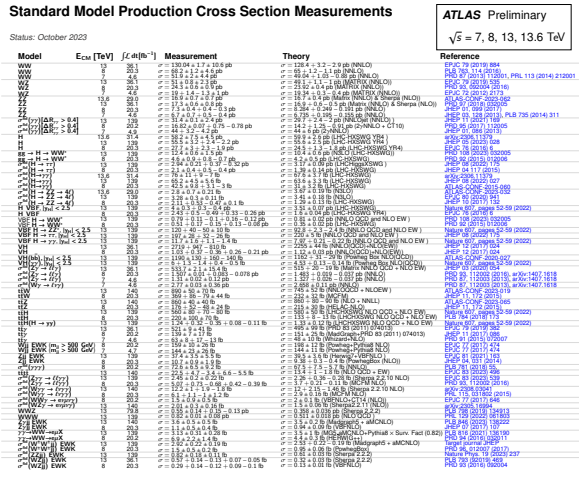

(c)

Figure 3: Summary of several Standard Model total and fiducial production cross-section measurements (a) with associated references (b) and (c). Where total cross sections are reported, the measurements are corrected for branching fractions and compared to the corresponding theoretical expectations. In some cases, the fiducial selection is different between measurements in the same final state for different centre-of-mass energies $\sqrt{s}$, resulting in lower cross section values at higher $\sqrt{s}$.

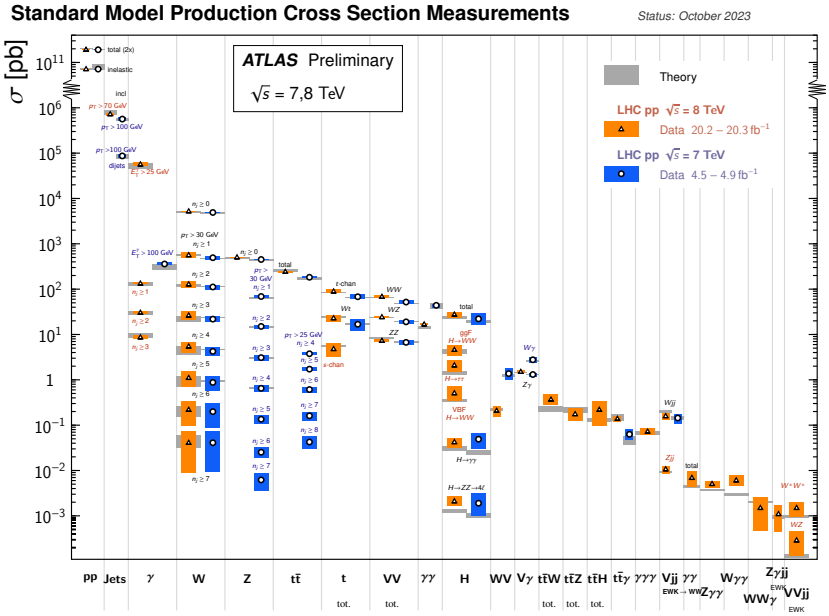

Figure 4: Summary of several Standard Model total and fiducial production cross-section measurements from Run 1. Where total cross sections are reported, the measurements are corrected for branching fractions and compared to the corresponding theoretical expectations. In some cases, the fiducial selection is different between measurements in the same final state for different centre-of-mass energies $\sqrt{s}$, resulting in lower cross section values at higher $\sqrt{s}$. The associated references can be found in Table 3(b) and 3(c).

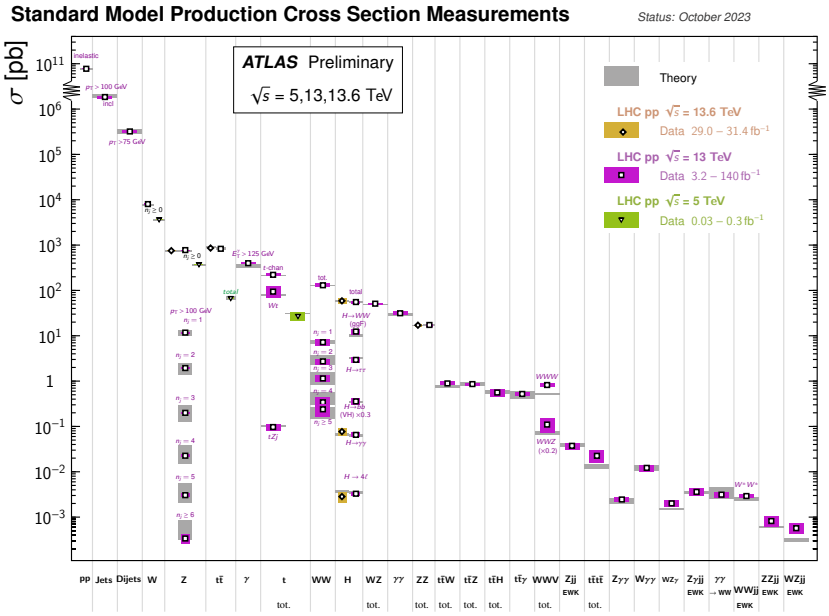

Figure 5: Summary of several Standard Model total and fiducial production cross-section measurements from Run 2 and 3. Where total cross sections are reported, the measurements are corrected for branching fractions and compared to the corresponding theoretical expectations. The associated references can be found in Table 3(b) and 3(c).

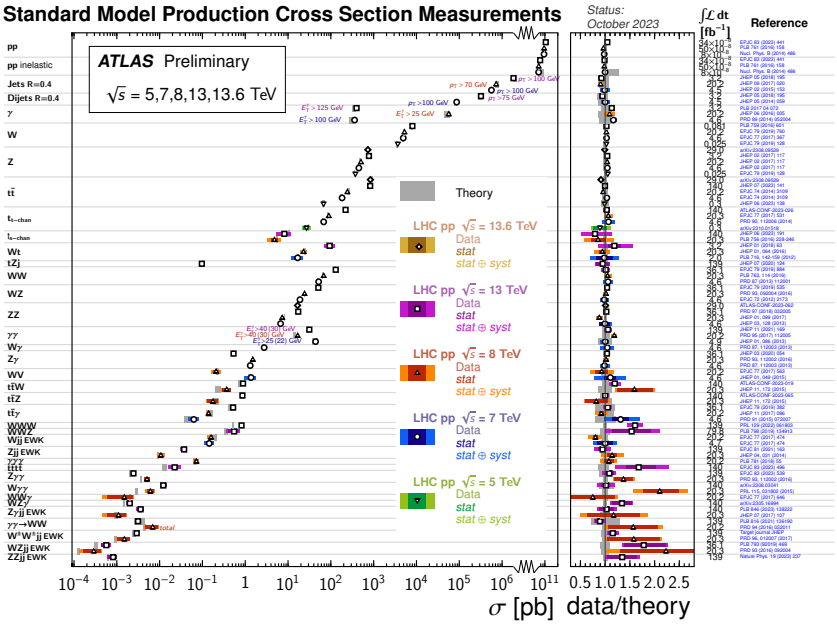

Figure 6: Summary of several Standard Model total and fiducial production cross-section measurements. Where total cross sections are reported, the measurements are corrected for branching fractions and compared to the corresponding theoretical expectations and ratio with respect to theory. In some cases, the fiducial selection is different between measurements in the same final state for different centre-of-mass energies $\sqrt{s}$, resulting in lower cross section values at higher $\sqrt{s}$.

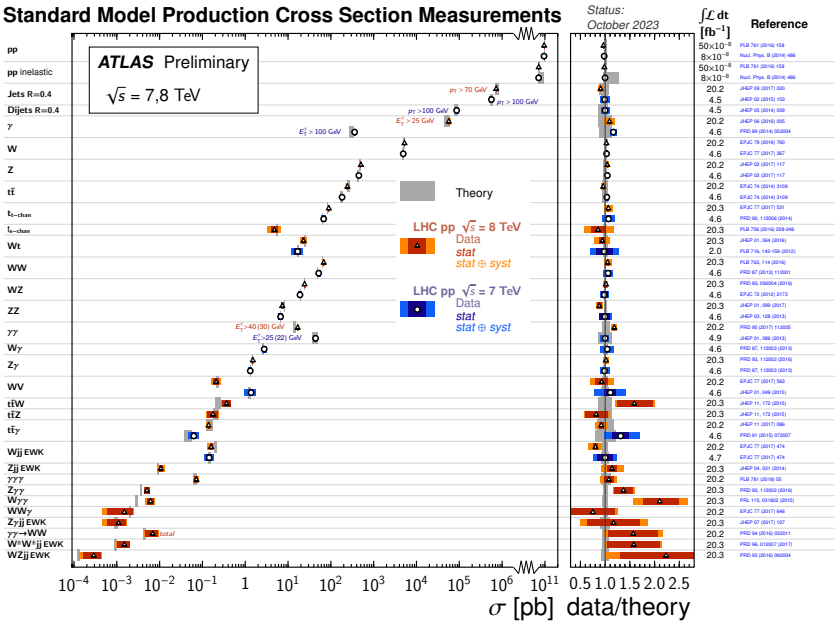

Figure 7: Summary of several Standard Model total and fiducial production cross-section measurements from Run 1. Where total cross sections are reported, the measurements are corrected for branching fractions and compared to the corresponding theoretical expectations and ratio with respect to theory. In some cases, the fiducial selection is different between measurements in the same final state for different centre-of-mass energies $\sqrt{s}$, resulting in lower cross section values at higher $\sqrt{s}$.

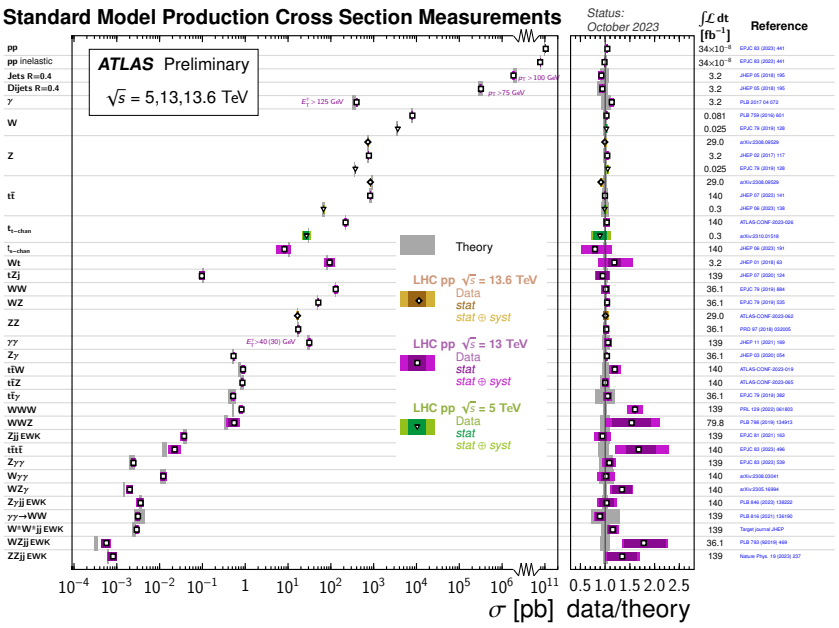

Figure 8: Summary of several Standard Model total and fiducial production cross-section measurements from Run 2 and 3 . Where total cross sections are reported, the measurements are corrected for branching fractions and compared to the corresponding theoretical expectations and ratio with respect to theory.

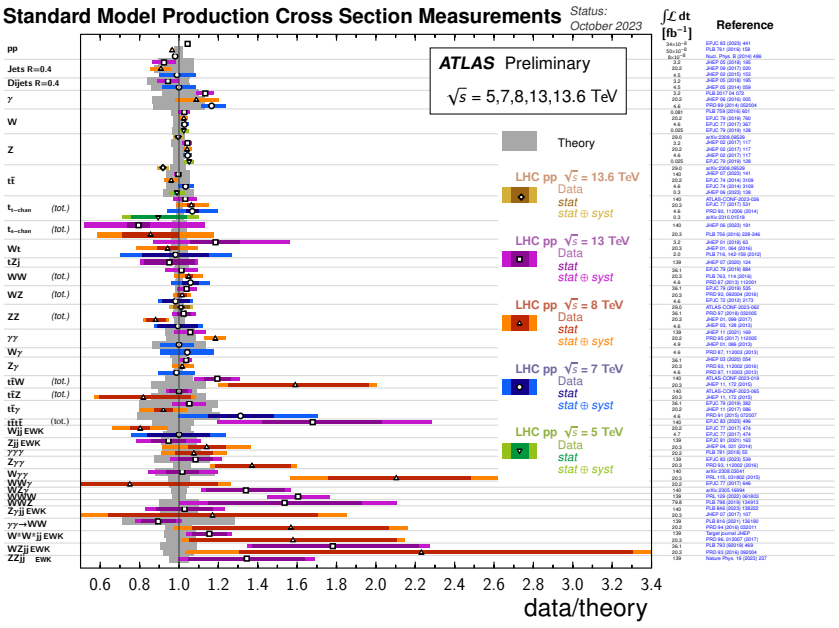

Figure 9: Summary of ratios with respect to theory for several Standard Model total and fiducial production cross-section measurements. Where total cross sections are reported, the measurements are corrected for branching fractions.

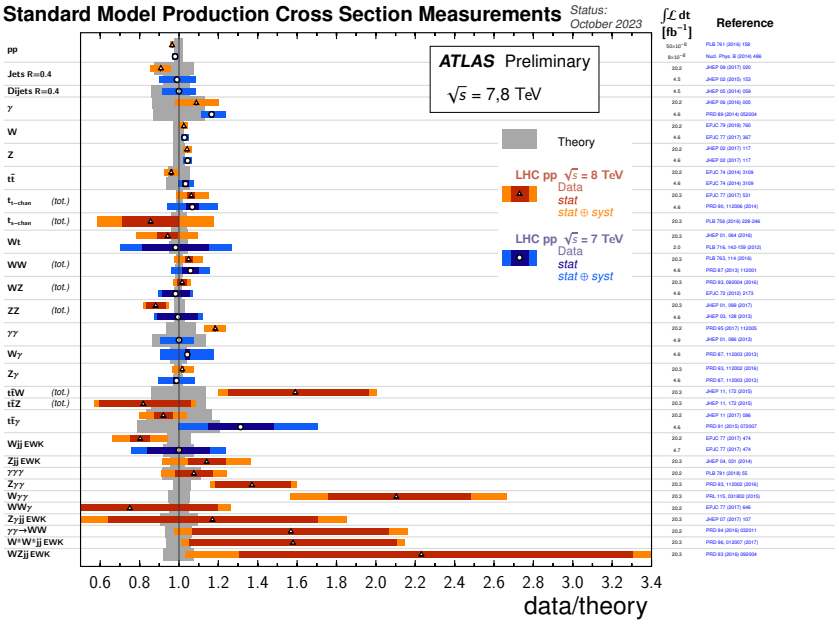

Figure 10: Summary of ratios with respect to theory for several Standard Model total and fiducial production cross-section measurements from Run 1. Where total cross sections are reported, the measurements are corrected for branching fractions.

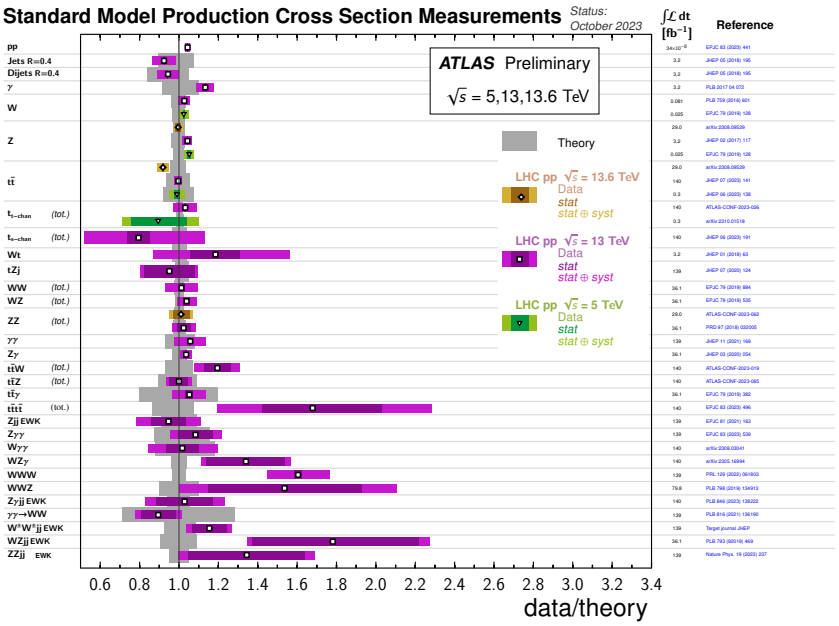

Figure 11: Summary of ratios with respect to theory for several Standard Model total and fiducial production cross-section measurements from Run 2 and 3. Where total cross sections are reported, the measurements are corrected for branching fractions.

5 Overview plots for inclusive measurements

Figures 12, 13, 14 show the data/theory ratio for several inclusive jet fiducial production cross-section measurements. All theoretical expectations were calculated at NLO or higher. The dark-color error bar represents the statistical uncertainty. The lighter-color error bar represents the full uncertainty, including systematics and luminosity uncertainties. The luminosity used and reference for each measurement are also shown. Uncertainties for the theoretical predictions are quoted from the original ATLAS papers.

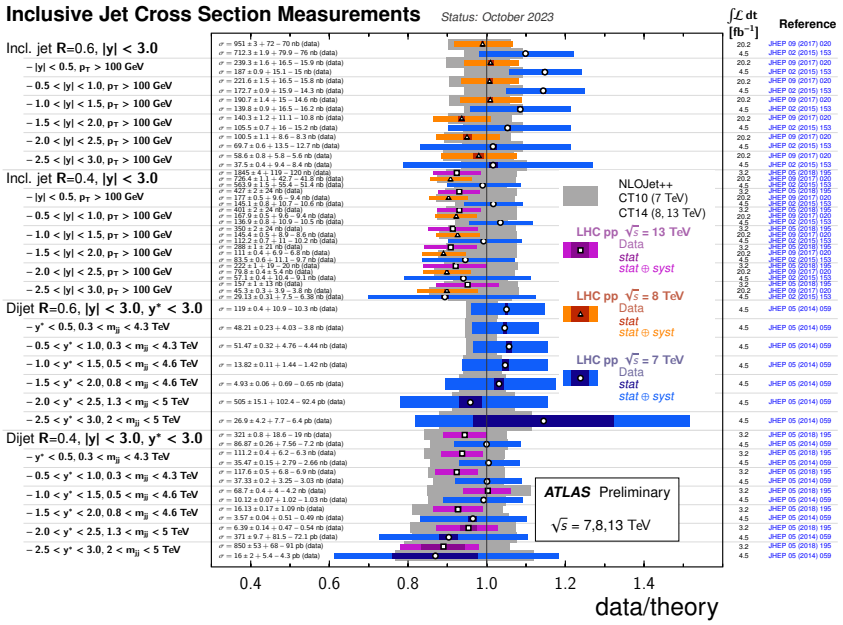

Figure 12: The data/theory ratio for several inclusive jet fiducial production cross-section measurements.

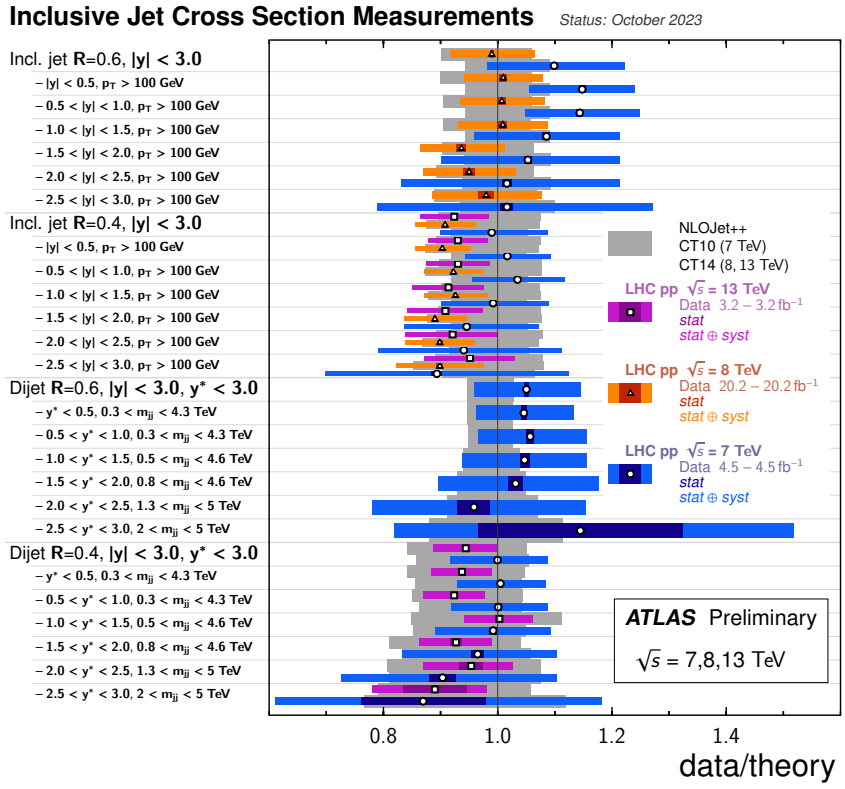

Figure 13: The data/theory ratio for several inclusive jet fiducial production cross-section measurements.

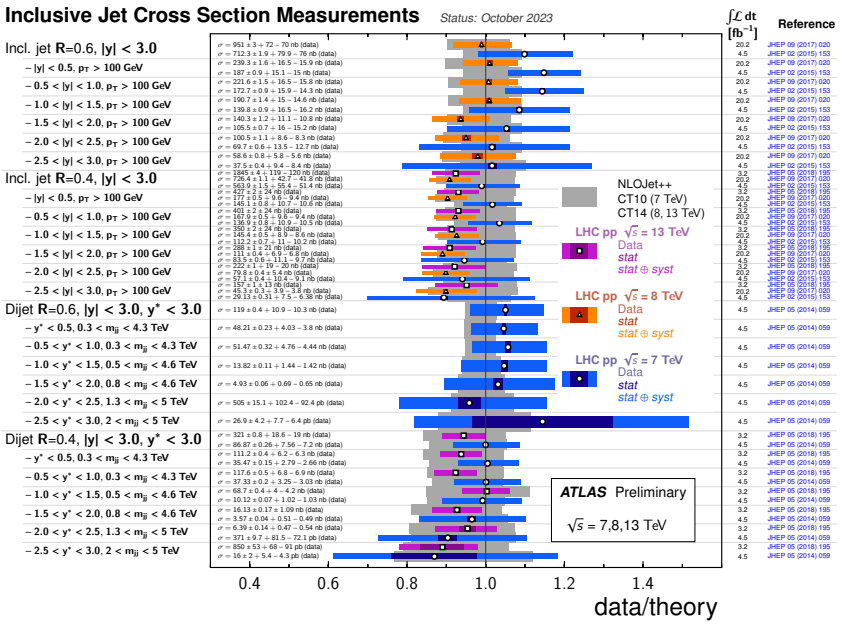

Figure 14: The ratio for several inclusive photon fiducial production cross-section measurements over theory prediction. All theoretical expectations are shown using gray bars, hatched for NLO calculations and full for NNLO predictions.

6 Overview plots for single boson measurements

Figures 15 and 16 show the data/theory ratio for several single-boson fiducial production cross-section measurements, corrected for branching fractions. All theoretical expectations were calculated at NLO or higher. The dark-color error bar represents the statistical uncertainly. The lighter-color error bar represents the full uncertainty, including systematics and luminosity uncertainties. The luminosity used and reference for each measurement are also shown. Uncertainties for the theoretical predictions are quoted from the original ATLAS papers. They were not always evaluated using the same prescriptions for PDFs and scales.

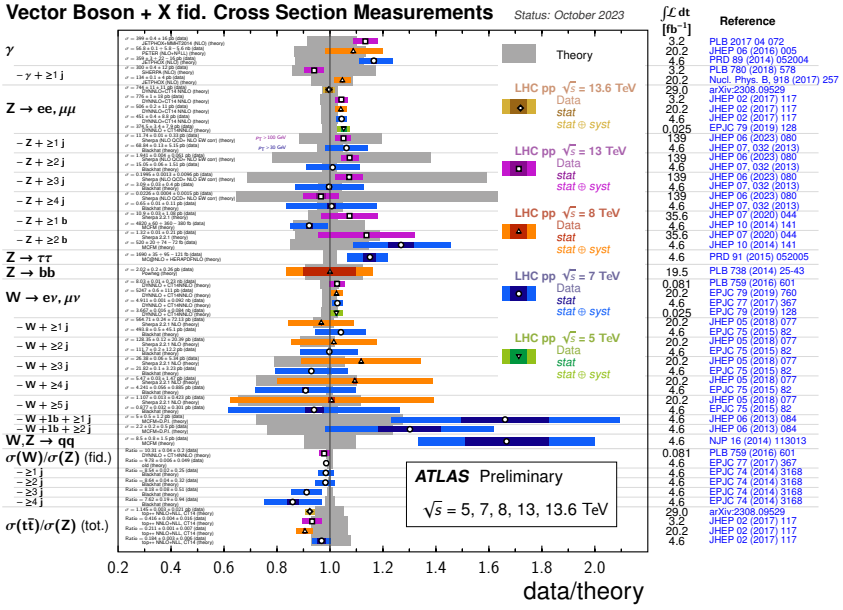

Figure 15: The data/theory ratio for several single-boson fiducial production cross-section measurements. Where total cross sections are reported, the measurements are corrected for branching fractions.

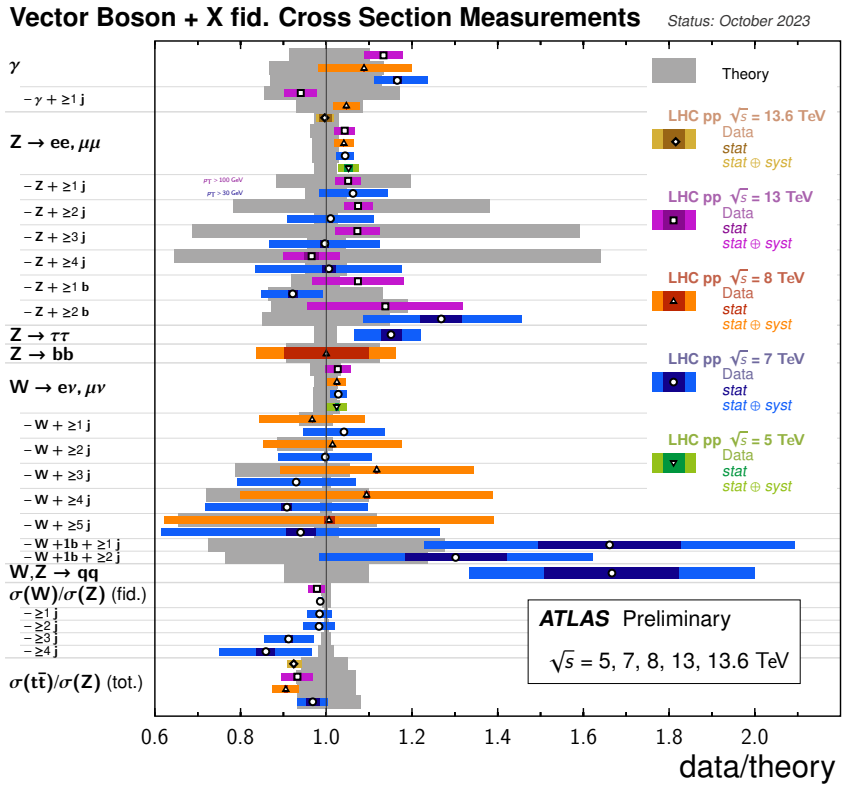

Figure 16: The data/theory ratio for several single-boson fiducial production cross-section measurements. Where total cross sections are reported, the measurements are corrected for branching fractions.

7 Overview plots for diboson measurements

Figures 17 and 18 show the ratio for several diboson total and fiducial production cross-section measurements over theory prediction, corrected for branching fractions. All theoretical expectations are shown using gray bars, hatched for NLO calculations and full for NNLO predictions. The dark-color error bar represents the statistical uncertainly. The lighter-color error bar represents the full uncertainty, including systematics and luminosity uncertainties. The luminosity used and reference for each measurement are also shown. Uncertainties for the theoretical predictions are quoted from the original ATLAS papers.

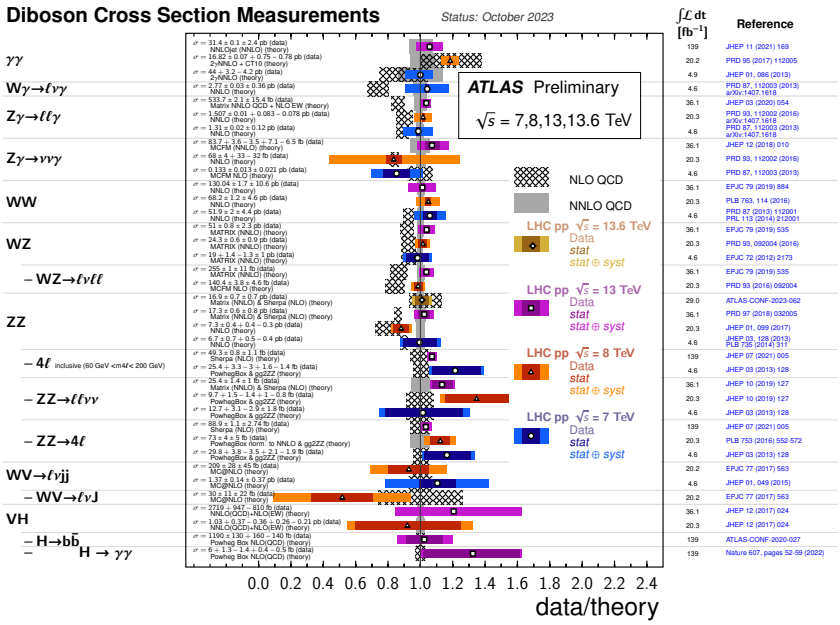

Figure 17: The data/theory ratio for several diboson fiducial production cross-section measurements. Where total cross sections are reported, the measurements are corrected for branching fractions.

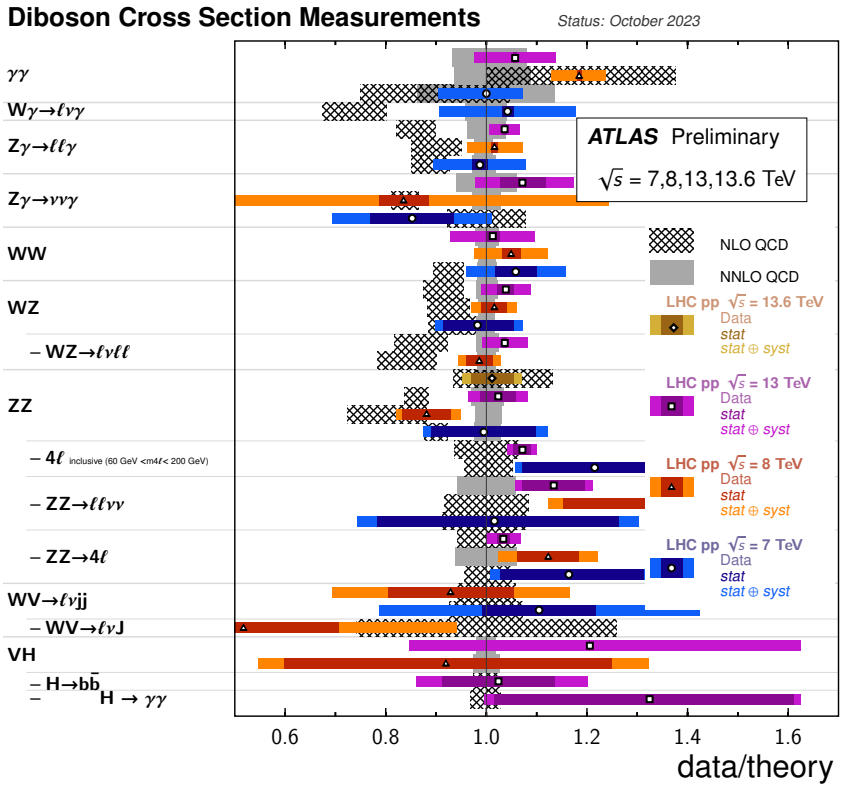

Figure 18: The data/theory ratio for several diboson fiducial production cross-section measurements. Where total cross sections are reported, the measurements are corrected for branching fractions.

8 Overview plots for VBF, VBS and triboson measurements

Figures 19 and 20 show the data/theory ratio for several vector boson fusion, vector boson scattering, and triboson fiducial cross-section measurements. The dark-color error bar represents the statistical uncertainty. The lighter-color error bar represents the full uncertainty, including systematics and luminosity uncertainties. The luminosity used and reference for each measurement are also shown. Uncertainties for the theoretical predictions are quoted from the original ATLAS papers. They were not always evaluated using the same prescriptions for PDFs and scales.

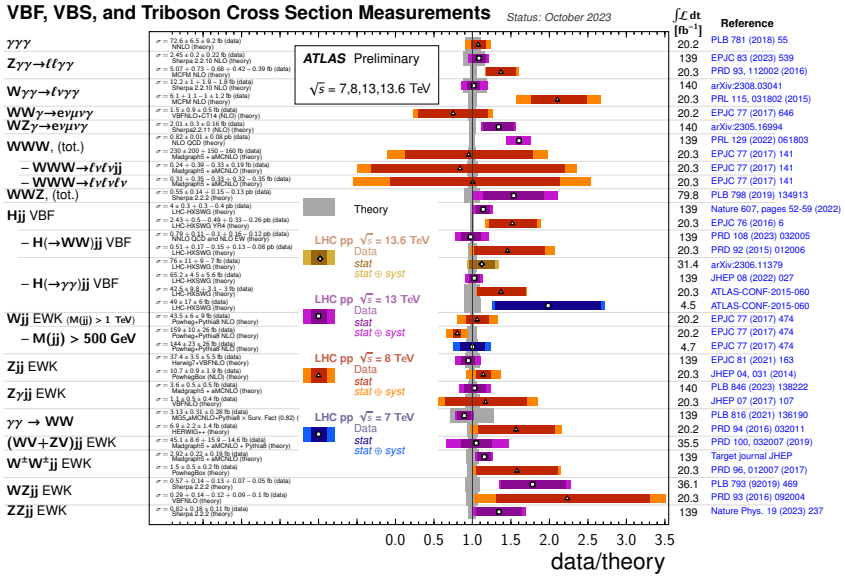

Figure 19: The data/theory ratio for several vector boson fusion, vector boson scattering, and triboson fiducial production cross-section measurements.

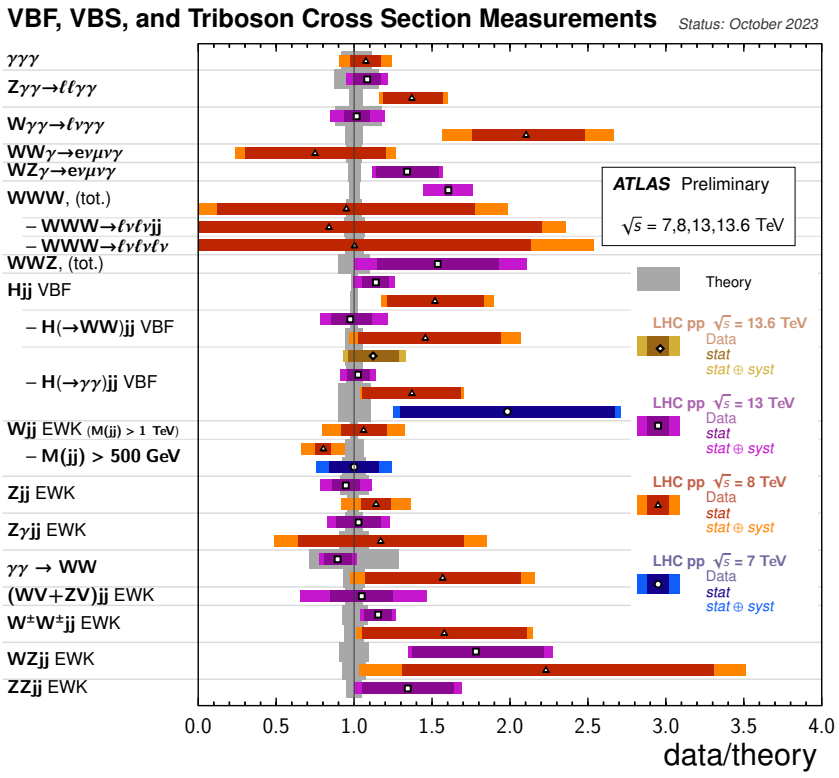

Figure 20: The data/theory ratio for several vector boson fusion, vector boson scattering, and triboson fiducial production cross-section measurements.

9 Used values

Figures 21, 23, 24, and 25 present tables of used results. Uncertainties for the theoretical predictions are quoted from the original ATLAS papers. They were not always evaluated using the same prescriptions for PDFs and scales.

Standard Model Production Cross Section Measurements I

Status: October 2023

ATLAS Preliminary
$\sqrt{s}$ = 7, 8, 13, 13.6 TeV

Model	E_{CM} [TeV]	$\int \mathcal{L}\, dt$[fb^{-1}]	Measurement	Theory	Reference
H	13.6	31.4	$\sigma = 58.2 \pm 7.5 \pm 4.5$ pb	$\sigma = 59.9 \pm 2.6$ pb (LHC-HXSWG YR4)	arXiv:2306.11379
H	13	139	$\sigma = 55.5 \pm 3.2 + 2.4 - 2.2$ pb	$\sigma = 55.6 \pm 2.5$ pb (LHC-HXSWG YR4)	JHEP 05 (2023) 028
H	8	20.3	$\sigma = 27.7 \pm 3 + 2.3 - 1.9$ pb	$\sigma = 24.5 + 1.3 - 1.8$ pb (LHC-HXSWG YR4)	EPJC 76 (2016) 6
H	7	4.5	$\sigma = 22.1 + 6.7 - 5.3 + 3.3 - 2.7$ pb	$\sigma = 19.2 + 1 - 1.4$ pb (LHC-HXSWG YR4)	EPJC 76 (2016) 6
H ggF, $\lvert y_H \rvert < 2.5$	13	139	$\sigma = 45.7 + 1.7 - 1.8 + 2.2 - 2.7$ pb	$\sigma = 44.8 \pm 2.6$ pb (LHC-HXSWG)	ATLAS-CONF-2021-053
H ggF	8	20.3	$\sigma = 23.9 \pm 3.1 + 2.1 - 1.9$ pb	$\sigma = 21.4 + 1.2 - 1.6$ pb (LHC-HXSWG YR4)	EPJC 76, 6 (2016)
H VBF, $\lvert y_H \rvert < 2.5$	13	139	$\sigma = 4 \pm 0.3 + 0.3 - 0.4$ pb	$\sigma = 3.51 \pm 0.07$ pb (LHC-HXSWG)	Nature 607, pages 52-59 (2022)
H VBF	8	20.3	$\sigma = 2.43 + 0.5 - 0.49 + 0.33 - 0.26$ pb	$\sigma = 1.6 \pm 0.04$ pb (LHC-HXSWG YR4)	EPJC 76 (2016) 6
WH, $\lvert y_H \rvert < 2.5$	13	139	$\sigma = 1.56 + 0.2 - 0.21 + 0.16 - 0.18$ pb	$\sigma = 1.203 \pm 0.024$ pb (Powheg Box NLO(QCD))	Nature 607, pages 52-59 (2022)
ZH, $\lvert y_H \rvert < 2.5$	13	139	$\sigma = 0.7 \pm 0.13 + 0.1 - 0.12$ pb	$\sigma = 0.795 \pm 0.03$ pb (Powheg Box NLO(QCD))	Nature 607, pages 52-59 (2022)
VH	13	36.1	$\sigma = 2719 + 947 - 810$ fb	$\sigma = 2255 \pm 44$ fb (NNLO(QCD)+NLO(EW))	JHEP 12 (2017) 024
VH	8	20.3	$\sigma = 1.03 + 0.37 - 0.36 + 0.26 - 0.21$ pb	$\sigma = 1.12 \pm 0.03$ pb (NNLO(QCD)+NLO(EW))	JHEP 12 (2017) 024
VH($b\bar{b}$), $\lvert y_H \rvert < 2.5$	13	139	$\sigma = 1190 \pm 130 + 160 - 140$ fb	$\sigma = 1162 + 31 - 29$ fb (Powheg Box NLO(QCD))	ATLAS-CONF-2020-027
VH($\gamma\gamma$), $\lvert y_H \rvert < 2.5$	13	139	$\sigma = 6 + 1.3 - 1.4 + 0.4 - 0.5$ fb	$\sigma = 4.53 + 0.13 - 0.14$ fb (Powheg Box NLO(QCD))	Nature 607, pages 52-59 (2022)
tt̄H	13	139	$\sigma = 560 \pm 80 + 70 - 80$ fb	$\sigma = 580 \pm 50$ fb (LHCHXSWG NLO QCD + NLO EW)	Nature 607, pages 52-59 (2022)
tt̄H	8	20.3	$\sigma = 220 \pm 100 \pm 70$ fb	$\sigma = 133 + 8 - 13$ fb (LHCHXSWG NLO QCD + NLO EW)	PLB 784 (2018) 173
σ^{fid}**(H→$\gamma\gamma$)**	13.6	31.4	$\sigma = 76 \pm 11 + 9 - 7$ fb	$\sigma = 67.6 \pm 3.7$ fb (LHC-HXSWG)	arXiv:2306.11379
σ^{fid}**(H→$\gamma\gamma$)**	13	139	$\sigma = 65.2 \pm 4.5 \pm 5.6$ fb	$\sigma = 63.6 \pm 3.3$ fb (LHC-HXSWG)	JHEP 08 (2022) 027
σ^{fid}**(H→$\gamma\gamma$)**	8	20.3	$\sigma = 42.5 \pm 9.8 + 3.1 - 3$ fb	$\sigma = 31 \pm 3.2$ fb (LHC-HXSWG)	ATLAS-CONF-2015-060
σ^{fid}**(H→$\gamma\gamma$)**	7	4.5	$\sigma = 49 \pm 17 \pm 6$ fb	$\sigma = 24.7 \pm 2.6$ fb (LHC-HXSWG)	ATLAS-CONF-2015-060
VBF **H → WW***	13	139	$\sigma = 0.79 + 0.11 - 0.1 + 0.16 - 0.12$ pb	$\sigma = 0.81 \pm 0.02$ pb (NNLO QCD and NLO EW)	PRD 108 (2023) 032005
VBF **H → WW***	8	20.3	$\sigma = 0.51 + 0.17 - 0.15 + 0.13 - 0.08$ pb	$\sigma = 0.35 \pm 0.02$ pb (LHC-HXSWG)	PRD 92 (2015) 012006
VBF H → ZZ*, $\lvert y_H \rvert < 2.5$	13	139	$\sigma = 120 + 40 - 50 \pm 10$ fb	$\sigma = 92.8 + 2.3 - 2.4$ fb (NNLO QCD and NLO EW)	Nature 607, pages 52-59 (2022)
VBF H → $\tau\tau$, $\lvert y_H \rvert < 2.5$	13	139	$\sigma = 197 \pm 28 + 32 - 26$ fb	$\sigma = 220 \pm 5$ fb (NNLO QCD and NLO EW)	JHEP 08 (2022) 175
VBF H → $\gamma\gamma$, $\lvert y_H \rvert < 2.5$	13	139	$\sigma = 11.7 \pm 1.6 + 1.1 - 1.4$ fb	$\sigma = 7.97 + 0.21 - 0.22$ fb (NNLO QCD and NLO EW)	Nature 607, pages 52-59 (2022)
gg → H → WW*	13	139	$\sigma = 12.4 \pm 0.6 \pm 1.5$ pb	$\sigma = 10.4 \pm 0.6$ pb (N3LO (LHC-HXSWG))	PRD 108 (2023) 032005
gg → H → WW*	8	20.3	$\sigma = 4.6 \pm 0.9 + 0.8 - 0.7$ pb	$\sigma = 4.2 \pm 0.5$ pb (LHC-HXSWG)	PRD 92 (2015) 012006
gg → H → WW*	7	4.5	$\sigma = 2 \pm 1.7 + 1.2 - 1.1$ pb	$\sigma = 3.3 \pm 0.4$ pb (LHC-HXSWG)	PRD 92 (2015) 012006
σ^{fid}**(H → ZZ → 4ℓ)**	13.6	29.0	$\sigma = 2.8 \pm 0.7 \pm 0.21$ fb	$\sigma = 3.67 \pm 0.19$ fb (N3LO)	ATLAS-CONF-2023-032
σ^{fid}**(H → ZZ → 4ℓ)**	13	139	$\sigma = 3.28 \pm 0.3 \pm 0.11$ fb	$\sigma = 3.41 \pm 0.18$ fb (N3LO)	EPJC 80 (2020) 941
σ^{fid}**(H → ZZ → 4ℓ)**	8	20.3	$\sigma = 2.11 + 0.53 - 0.47 \pm 0.1$ fb	$\sigma = 1.29 \pm 0.13$ fb (LHC-HXSWG)	JHEP 10 (2017) 132
σ^{fid}**(H → ZZ → 4ℓ)**	7	4.5	$\sigma = 1.9 + 1.2 - 0.9 \pm 0.1$ fb	$\sigma = 1.03 \pm 0.11$ fb (LHC-HXSWG)	JHEP 10 (2017) 132
σ^{fid}**(H → $\tau\tau$)**	13	139	$\sigma = 2.94 \pm 0.21 + 0.37 - 0.32$ pb	$\sigma = 3.17 \pm 0.09$ pb (LHCHiggsXSWG)	JHEP 08 (2022) 175
σ^{fid}**(H → $\tau\tau$)**	8	20.3	$\sigma = 2.1 \pm 0.4 + 0.5 - 0.4$ pb	$\sigma = 1.39 \pm 0.14$ pb (LHC-HXSWG)	JHEP 04 117 (2015)
σ^{fid}**(H → $\tau\tau$)**	7	4.5	$\sigma = 1 + 0.9 - 0.8 + 0.9 - 0.8$ pb	$\sigma = 1.09 \pm 0.11$ pb (LHC-HXSWG)	JHEP 04 117 (2015)

Figure 21: Measured cross-sections and associated predictions for the Higgs results displayed in all figures.

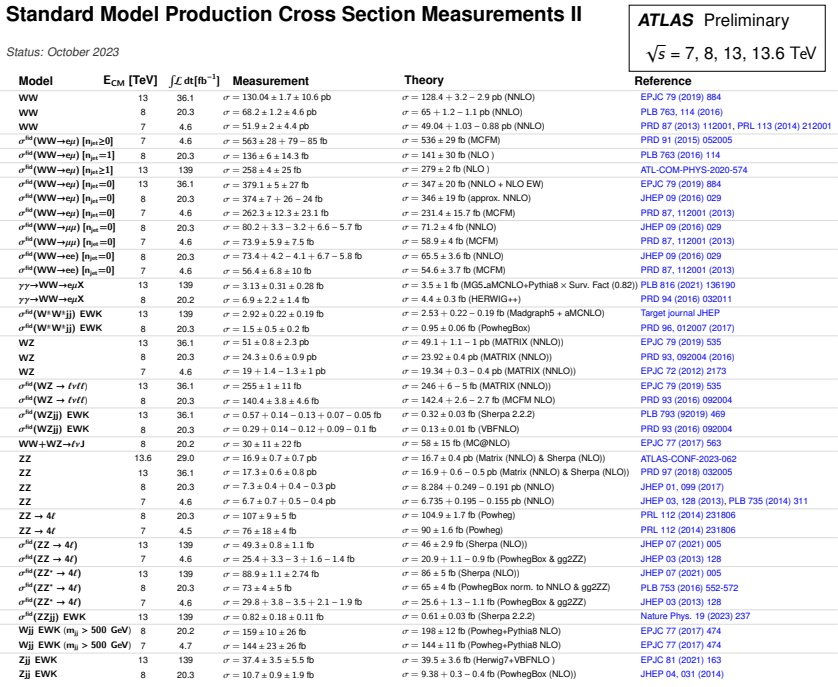

Standard Model Production Cross Section Measurements II

Status: October 2023

ATLAS Preliminary

$\sqrt{s}$ = 7, 8, 13, 13.6 TeV

Model	E_{CM} [TeV]	$\int \mathcal{L}\,dt$[fb^{-1}]	Measurement	Theory	Reference
WW	13	36.1	$\sigma = 130.04 \pm 1.7 \pm 10.6$ pb	$\sigma = 128.4 + 3.2 - 2.9$ pb (NNLO)	EPJC 79 (2019) 884
WW	8	20.3	$\sigma = 68.2 \pm 1.2 \pm 4.6$ pb	$\sigma = 65 + 1.2 - 1.1$ pb (NNLO)	PLB 763, 114 (2016)
WW	7	4.6	$\sigma = 51.9 \pm 2 \pm 4.4$ pb	$\sigma = 49.04 + 1.03 - 0.88$ pb (NNLO)	PRD 87 (2013) 112001, PRL 113 (2014) 212001
σ^{fid}(WW→eμ) [n_{jet}=0]	7	4.6	$\sigma = 563 \pm 28 + 79 - 85$ fb	$\sigma = 536 \pm 29$ fb (MCFM)	PRD 91 (2015) 052005
σ^{fid}(WW→eμ) [n_{jet}=1]	8	20.3	$\sigma = 136 \pm 6 \pm 14.3$ fb	$\sigma = 141 \pm 30$ fb (NLO)	PLB 763 (2016) 114
σ^{fid}(WW→eμ) [n_{jet}≥1]	13	139	$\sigma = 258 \pm 4 \pm 25$ fb	$\sigma = 279 \pm 2$ fb (NLO)	ATL-COM-PHYS-2020-574
σ^{fid}(WW→eμ) [n_{jet}=0]	13	36.1	$\sigma = 379.1 \pm 5 \pm 27$ fb	$\sigma = 347 \pm 20$ fb (NNLO + NLO EW)	EPJC 79 (2019) 884
σ^{fid}(WW→eμ) [n_{jet}=0]	8	20.3	$\sigma = 374 \pm 7 + 26 - 24$ fb	$\sigma = 346 \pm 19$ fb (approx. NNLO)	JHEP 09 (2016) 029
σ^{fid}(WW→eμ) [n_{jet}=0]	7	4.6	$\sigma = 262.3 \pm 12.3 \pm 23.1$ fb	$\sigma = 231.4 \pm 15.7$ fb (MCFM)	PRD 87, 112001 (2013)
σ^{fid}(WW→μμ) [n_{jet}=0]	8	20.3	$\sigma = 80.2 + 3.3 - 3.2 + 6.6 - 5.7$ fb	$\sigma = 71.2 \pm 4$ fb (NNLO)	JHEP 09 (2016) 029
σ^{fid}(WW→μμ) [n_{jet}=0]	7	4.6	$\sigma = 73.9 \pm 5.9 \pm 7.5$ fb	$\sigma = 58.9 \pm 4$ fb (MCFM)	PRD 87, 112001 (2013)
σ^{fid}(WW→ee) [n_{jet}=0]	8	20.3	$\sigma = 73.4 + 4.2 - 4.1 + 6.7 - 5.8$ fb	$\sigma = 65.5 \pm 3.6$ fb (NNLO)	JHEP 09 (2016) 029
σ^{fid}(WW→ee) [n_{jet}=0]	7	4.6	$\sigma = 56.4 \pm 6.8 \pm 10$ fb	$\sigma = 54.6 \pm 3.7$ fb (MCFM)	PRD 87, 112001 (2013)
γγ→WW→eμX	13	139	$\sigma = 3.13 \pm 0.31 \pm 0.28$ fb	$\sigma = 3.5 \pm 1$ fb (MG5_aMCNLO+Pythia8 × Surv. Fact (0.82))	PLB 816 (2021) 136190
γγ→WW→eμX	8	20.2	$\sigma = 6.9 \pm 2.2 \pm 1.4$ fb	$\sigma = 4.4 \pm 0.3$ fb (HERWIG++)	PRD 94 (2016) 032011
σ^{fid}(W±W±jj) EWK	13	139	$\sigma = 2.92 \pm 0.22 \pm 0.19$ fb	$\sigma = 2.53 + 0.22 - 0.19$ fb (Madgraph5 + aMCNLO)	Target journal JHEP
σ^{fid}(W±W±jj) EWK	8	20.3	$\sigma = 1.5 \pm 0.5 \pm 0.2$ fb	$\sigma = 0.95 \pm 0.06$ fb (PowhegBox)	PRD 96, 012007 (2017)
WZ	13	36.1	$\sigma = 51 \pm 0.8 \pm 2.3$ pb	$\sigma = 49.1 + 1.1 - 1$ pb (MATRIX (NNLO))	EPJC 79 (2019) 535
WZ	8	20.3	$\sigma = 24.3 \pm 0.6 \pm 0.9$ pb	$\sigma = 23.92 \pm 0.4$ pb (MATRIX (NNLO))	PRD 93, 092004 (2016)
WZ	7	4.6	$\sigma = 19 + 1.4 - 1.3 \pm 1$ pb	$\sigma = 19.34 + 0.3 - 0.4$ pb (MATRIX (NNLO))	EPJC 72 (2012) 2173
σ^{fid}(WZ → $\ell\nu\ell\ell$)	13	36.1	$\sigma = 255 \pm 1 \pm 11$ fb	$\sigma = 246 + 6 - 5$ fb (MATRIX (NNLO))	EPJC 79 (2019) 535
σ^{fid}(WZ → $\ell\nu\ell\ell$)	8	20.3	$\sigma = 140.4 \pm 3.8 \pm 4.6$ fb	$\sigma = 142.4 + 2.6 - 2.7$ fb (MCFM NLO)	PRD 93 (2016) 092004
σ^{fid}(WZjj) EWK	13	36.1	$\sigma = 0.57 + 0.14 - 0.13 + 0.07 - 0.05$ fb	$\sigma = 0.32 \pm 0.03$ fb (Sherpa 2.2.2)	PLB 793 (92019) 469
σ^{fid}(WZjj) EWK	8	20.3	$\sigma = 0.29 + 0.14 - 0.12 + 0.09 - 0.1$ fb	$\sigma = 0.13 \pm 0.01$ fb (VBFNLO)	PRD 93 (2016) 092004
WW+WZ→$\ell\nu$J	8	20.2	$\sigma = 30 \pm 11 \pm 22$ fb	$\sigma = 58 \pm 15$ fb (MC@NLO)	EPJC 77 (2017) 563
ZZ	13.6	29.0	$\sigma = 16.9 \pm 0.7 \pm 0.7$ pb	$\sigma = 16.7 \pm 0.4$ pb (Matrix (NNLO) & Sherpa (NLO))	ATLAS-CONF-2023-062
ZZ	13	36.1	$\sigma = 17.3 \pm 0.6 \pm 0.8$ pb	$\sigma = 16.9 + 0.6 - 0.5$ pb (Matrix (NNLO) & Sherpa (NLO))	PRD 97 (2018) 032005
ZZ	8	20.3	$\sigma = 7.3 \pm 0.4 + 0.4 - 0.3$ pb	$\sigma = 8.284 + 0.249 - 0.191$ pb (NNLO)	JHEP 01, 099 (2017)
ZZ	7	4.6	$\sigma = 6.7 \pm 0.7 + 0.5 - 0.4$ pb	$\sigma = 6.735 + 0.195 - 0.155$ pb (NNLO)	JHEP 03, 128 (2013), PLB 735 (2014) 311
ZZ → 4ℓ	8	20.3	$\sigma = 107 \pm 9 \pm 5$ fb	$\sigma = 104.9 \pm 1.7$ fb (Powheg)	PRL 112 (2014) 231806
ZZ → 4ℓ	7	4.5	$\sigma = 76 \pm 18 \pm 4$ fb	$\sigma = 90 \pm 1.6$ fb (Powheg)	PRL 112 (2014) 231806
σ^{fid}(ZZ → 4ℓ)	13	139	$\sigma = 49.3 \pm 0.8 \pm 1.1$ fb	$\sigma = 46 \pm 2.9$ fb (Sherpa (NLO))	JHEP 07 (2021) 005
σ^{fid}(ZZ → 4ℓ)	7	4.6	$\sigma = 25.4 + 3.3 - 3 + 1.6 - 1.4$ fb	$\sigma = 20.9 + 1.1 - 0.9$ fb (PowhegBox & gg2ZZ)	JHEP 03 (2013) 128
σ^{fid}(ZZ* → 4ℓ)	13	139	$\sigma = 88.9 \pm 1.1 \pm 2.74$ fb	$\sigma = 86 \pm 5$ fb (Sherpa (NLO))	JHEP 07 (2021) 005
σ^{fid}(ZZ* → 4ℓ)	8	20.3	$\sigma = 73 \pm 4 \pm 5$ fb	$\sigma = 65 \pm 4$ fb (PowhegBox norm. to NNLO & gg2ZZ)	PLB 753 (2016) 552-572
σ^{fid}(ZZ* → 4ℓ)	7	4.6	$\sigma = 29.8 + 3.8 - 3.5 + 2.1 - 1.9$ fb	$\sigma = 25.6 + 1.3 - 1.1$ fb (PowhegBox & gg2ZZ)	JHEP 03 (2013) 128
σ^{fid}(ZZjj) EWK	13	139	$\sigma = 0.82 \pm 0.18 \pm 0.11$ fb	$\sigma = 0.61 \pm 0.03$ fb (Sherpa 2.2.2)	Nature Phys. 19 (2023) 237
Wjj EWK (m_{jj} > 500 GeV)	8	20.2	$\sigma = 159 \pm 10 \pm 26$ fb	$\sigma = 198 \pm 12$ fb (Powheg+Pythia8 NLO)	EPJC 77 (2017) 474
Wjj EWK (m_{jj} > 500 GeV)	7	4.7	$\sigma = 144 \pm 23 \pm 26$ fb	$\sigma = 144 \pm 11$ fb (Powheg+Pythia8 NLO)	EPJC 77 (2017) 474
Zjj EWK	13	139	$\sigma = 37.4 \pm 3.5 \pm 5.5$ fb	$\sigma = 39.5 \pm 3.6$ fb (Herwig7+VBFNLO)	EPJC 81 (2021) 163
Zjj EWK	8	20.3	$\sigma = 10.7 \pm 0.9 \pm 1.9$ fb	$\sigma = 9.38 + 0.3 - 0.4$ fb (PowhegBox (NLO))	JHEP 04, 031 (2014)

Figure 22: Measured cross-sections and associated predictions for the Bosons results displayed in all figures.

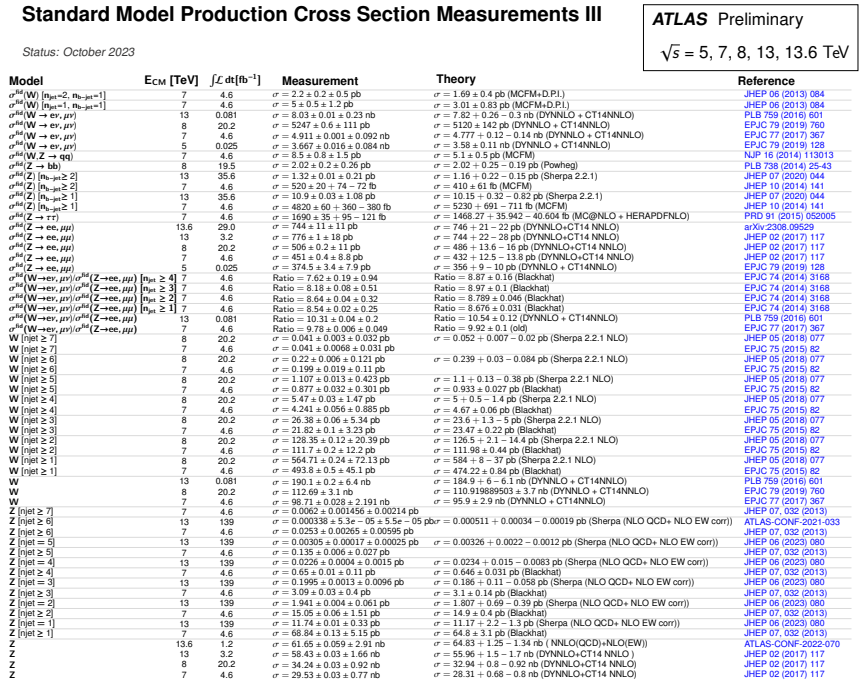

Standard Model Production Cross Section Measurements III

Status: October 2023

ATLAS Preliminary

$\sqrt{s}$ = 5, 7, 8, 13, 13.6 TeV

Model	E_{CM} [TeV]	$\int \mathcal{L}\,dt$[fb^{-1}]	Measurement	Theory	Reference
σ^{fid}(W) [n_{jet}=2, n_{b-jet}=1]	7	4.6	$\sigma = 2.2 \pm 0.2 \pm 0.5$ pb	$\sigma = 1.69 \pm 0.4$ pb (MCFM+D.P.I.)	JHEP 06 (2013) 084
σ^{fid}(W) [n_{jet}=1, n_{b-jet}=1]	7	4.6	$\sigma = 5 \pm 0.5 \pm 1.2$ pb	$\sigma = 3.01 \pm 0.83$ pb (MCFM+D.P.I.)	JHEP 06 (2013) 084
σ^{fid}(W → eν, μν)	13	0.081	$\sigma = 8.03 \pm 0.01 \pm 0.23$ nb	$\sigma = 7.82 + 0.26 - 0.3$ nb (DYNNLO + CT14NNLO)	PLB 759 (2016) 601
σ^{fid}(W → eν, μν)	8	20.2	$\sigma = 5247 \pm 0.6 \pm 111$ pb	$\sigma = 5120 \pm 142$ pb (DYNNLO + CT14NNLO)	EPJC 79 (2019) 760
σ^{fid}(W → eν, μν)	7	4.6	$\sigma = 4.911 \pm 0.001 \pm 0.092$ nb	$\sigma = 4.777 + 0.12 - 0.14$ nb (DYNNLO + CT14NNLO)	EPJC 77 (2017) 367
σ^{fid}(W → eν, μν)	5	0.025	$\sigma = 3.667 \pm 0.016 \pm 0.084$ nb	$\sigma = 3.58 \pm 0.11$ nb (DYNNLO + CT14NNLO)	EPJC 79 (2019) 128
σ^{fid}(W,Z → qq)	7	4.6	$\sigma = 8.5 \pm 0.8 \pm 1.5$ pb	$\sigma = 5.1 \pm 0.5$ pb (MCFM)	NJP 16 (2014) 113013
σ^{fid}(Z → bb)	8	19.5	$\sigma = 2.02 \pm 0.2 \pm 0.26$ pb	$\sigma = 2.02 + 0.25 - 0.19$ pb (Powheg)	PLB 738 (2014) 25-43
σ^{fid}(Z) [$n_{b-jet} \geq 2$]	13	35.6	$\sigma = 1.32 \pm 0.01 \pm 0.21$ pb	$\sigma = 1.16 + 0.22 - 0.15$ pb (Sherpa 2.2.1)	JHEP 07 (2020) 044
σ^{fid}(Z) [$n_{b-jet} \geq 2$]	7	4.6	$\sigma = 520 \pm 20 + 74 - 72$ fb	$\sigma = 410 \pm 61$ fb (MCFM)	JHEP 10 (2014) 141
σ^{fid}(Z) [$n_{b-jet} \geq 1$]	13	35.6	$\sigma = 10.9 \pm 0.03 \pm 1.08$ pb	$\sigma = 10.15 + 0.32 - 0.82$ pb (Sherpa 2.2.1)	JHEP 07 (2020) 044
σ^{fid}(Z) [$n_{b-jet} \geq 1$]	7	4.6	$\sigma = 4820 \pm 60 + 360 - 380$ fb	$\sigma = 5230 \pm 691 - 711$ fb (MCFM)	JHEP 10 (2014) 141
σ^{fid}(Z → ττ)	7	4.6	$\sigma = 1690 \pm 35 + 95 - 121$ fb	$\sigma = 1468.27 \pm 35.942 - 40.604$ fb (MC@NLO + HERAPDFNLO)	PRD 91 (2015) 052005
σ^{fid}(Z → ee, μμ)	13.6	29.0	$\sigma = 744 \pm 11 \pm 11$ pb	$\sigma = 746 + 21 - 22$ pb (DYNNLO+CT14 NNLO)	arXiv:2308.09529
σ^{fid}(Z → ee, μμ)	13	3.2	$\sigma = 776 \pm 1 \pm 18$ pb	$\sigma = 744 + 22 - 28$ pb (DYNNLO+CT14 NNLO)	JHEP 02 (2017) 117
σ^{fid}(Z → ee, μμ)	8	20.2	$\sigma = 506 \pm 0.2 \pm 11$ pb	$\sigma = 486 + 13.6 - 16$ pb (DYNNLO+CT14 NNLO)	JHEP 02 (2017) 117
σ^{fid}(Z → ee, μμ)	7	4.6	$\sigma = 451 \pm 0.4 \pm 8.8$ pb	$\sigma = 432 + 12.5 - 13.8$ pb (DYNNLO+CT14 NNLO)	JHEP 02 (2017) 117
σ^{fid}(Z → ee, μμ)	5	0.025	$\sigma = 374.5 \pm 3.4 \pm 7.9$ pb	$\sigma = 356 \pm 9 - 10$ pb (DYNNLO + CT14NNLO)	EPJC 79 (2019) 128
σ^{fid}(W→eν, μν)/σ^{fid}(Z→ee,μμ) [$n_{jet} \geq 4$]	7	4.6	Ratio = $7.62 \pm 0.19 \pm 0.94$	Ratio = 8.87 ± 0.16 (Blackhat)	EPJC 74 (2014) 3168
σ^{fid}(W→eν, μν)/σ^{fid}(Z→ee,μμ) [$n_{jet} \geq 3$]	7	4.6	Ratio = $8.18 \pm 0.08 \pm 0.51$	Ratio = 8.97 ± 0.1 (Blackhat)	EPJC 74 (2014) 3168
σ^{fid}(W→eν, μν)/σ^{fid}(Z→ee,μμ) [$n_{jet} \geq 2$]	7	4.6	Ratio = $8.64 \pm 0.04 \pm 0.32$	Ratio = 8.789 ± 0.046 (Blackhat)	EPJC 74 (2014) 3168
σ^{fid}(W→eν, μν)/σ^{fid}(Z→ee,μμ) [$n_{jet} \geq 1$]	7	4.6	Ratio = $8.54 \pm 0.02 \pm 0.25$	Ratio = 8.676 ± 0.031 (Blackhat)	EPJC 74 (2014) 3168
σ^{fid}(W→eν, μν)/σ^{fid}(Z→ee,μμ)	13	0.081	Ratio = $10.31 \pm 0.04 \pm 0.2$	Ratio = 10.54 ± 0.12 (DYNNLO + CT14NNLO)	PLB 759 (2016) 601
σ^{fid}(W→eν, μν)/σ^{fid}(Z→ee,μμ)	7	4.6	Ratio = $9.78 \pm 0.006 \pm 0.049$	Ratio = 9.92 ± 0.1 (old)	EPJC 77 (2017) 367
W [njet ≥ 7]	8	20.2	$\sigma = 0.041 \pm 0.003 \pm 0.032$ pb	$\sigma = 0.052 + 0.007 - 0.02$ pb (Sherpa 2.2.1 NLO)	JHEP 05 (2018) 077
W [njet ≥ 7]	7	4.6	$\sigma = 0.041 \pm 0.0068 \pm 0.031$ pb		EPJC 75 (2015) 82
W [njet ≥ 6]	8	20.2	$\sigma = 0.22 \pm 0.006 \pm 0.121$ pb	$\sigma = 0.239 + 0.03 - 0.084$ pb (Sherpa 2.2.1 NLO)	JHEP 05 (2018) 077
W [njet ≥ 6]	7	4.6	$\sigma = 0.199 \pm 0.019 \pm 0.11$ pb		EPJC 75 (2015) 82
W [njet ≥ 5]	8	20.2	$\sigma = 1.107 \pm 0.013 \pm 0.423$ pb	$\sigma = 1.1 + 0.13 - 0.38$ pb (Sherpa 2.2.1 NLO)	JHEP 05 (2018) 077
W [njet ≥ 5]	7	4.6	$\sigma = 0.877 \pm 0.032 \pm 0.301$ pb	$\sigma = 0.933 \pm 0.027$ pb (Blackhat)	EPJC 75 (2015) 82
W [njet ≥ 4]	8	20.2	$\sigma = 5.47 \pm 0.03 \pm 1.47$ pb	$\sigma = 5 + 0.5 - 1.4$ pb (Sherpa 2.2.1 NLO)	JHEP 05 (2018) 077
W [njet ≥ 4]	7	4.6	$\sigma = 4.241 \pm 0.056 \pm 0.885$ pb	$\sigma = 4.67 \pm 0.06$ pb (Blackhat)	EPJC 75 (2015) 82
W [njet ≥ 3]	8	20.2	$\sigma = 26.38 \pm 0.06 \pm 5.34$ pb	$\sigma = 23.6 + 1.3 - 5$ pb (Sherpa 2.2.1 NLO)	JHEP 05 (2018) 077
W [njet ≥ 3]	7	4.6	$\sigma = 21.82 \pm 0.1 \pm 3.23$ pb	$\sigma = 23.47 \pm 0.22$ pb (Blackhat)	EPJC 75 (2015) 82
W [njet ≥ 2]	8	20.2	$\sigma = 128.35 \pm 0.12 \pm 20.39$ pb	$\sigma = 126.5 + 2.1 - 14.4$ pb (Sherpa 2.2.1 NLO)	JHEP 05 (2018) 077
W [njet ≥ 2]	7	4.6	$\sigma = 111.7 \pm 0.2 \pm 12.2$ pb	$\sigma = 111.98 \pm 0.44$ pb (Blackhat)	EPJC 75 (2015) 82
W [njet ≥ 1]	8	20.2	$\sigma = 564.71 \pm 0.24 \pm 72.13$ pb	$\sigma = 584 + 8 - 37$ pb (Sherpa 2.2.1 NLO)	JHEP 05 (2018) 077
W [njet ≥ 1]	7	4.6	$\sigma = 493.8 \pm 0.5 \pm 45.1$ pb	$\sigma = 474.22 \pm 0.84$ pb (Blackhat)	EPJC 75 (2015) 82
W	13	0.081	$\sigma = 190.1 \pm 0.2 \pm 6.4$ nb	$\sigma = 184.9 + 6 - 6.1$ nb (DYNNLO + CT14NNLO)	PLB 759 (2016) 601
W	8	20.2	$\sigma = 112.69 \pm 3.1$ nb	$\sigma = 110.919899503 \pm 3.7$ nb (DYNNLO + CT14NNLO)	EPJC 79 (2019) 760
W	7	4.6	$\sigma = 98.71 \pm 0.028 \pm 2.191$ nb	$\sigma = 95.9 \pm 2.9$ nb (DYNNLO + CT14NNLO)	EPJC 77 (2017) 367
Z [njet ≥ 7]	7	4.6	$\sigma = 0.0062 \pm 0.001456 \pm 0.00214$ pb		JHEP 07, 032 (2013)
Z [njet ≥ 6]	13	139	$\sigma = 0.000338 \pm 5.3e-05 \pm 5.5e-05$ pb	$\sigma = 0.000511 + 0.00034 - 0.00019$ pb (Sherpa (NLO QCD+ NLO EW corr))	ATLAS-CONF-2021-033
Z [njet ≥ 6]	7	4.6	$\sigma = 0.0253 \pm 0.00205 \pm 0.00595$ pb		JHEP 07, 032 (2013)
Z [njet = 5]	13	139	$\sigma = 0.00305 \pm 0.00017 \pm 0.00025$ pb	$\sigma = 0.00326 + 0.0022 - 0.0012$ pb (Sherpa (NLO QCD+ NLO EW corr))	JHEP 06 (2023) 080
Z [njet ≥ 5]	7	4.6	$\sigma = 0.135 \pm 0.006 \pm 0.027$ pb		JHEP 07, 032 (2013)
Z [njet = 4]	13	139	$\sigma = 0.0226 \pm 0.0004 \pm 0.0015$ pb	$\sigma = 0.0234 + 0.015 - 0.0083$ pb (Sherpa (NLO QCD+ NLO EW corr))	JHEP 06 (2023) 080
Z [njet ≥ 4]	7	4.6	$\sigma = 0.65 \pm 0.01 \pm 0.11$ pb	$\sigma = 0.646 \pm 0.031$ pb (Blackhat)	JHEP 07, 032 (2013)
Z [njet = 3]	13	139	$\sigma = 0.1995 \pm 0.0013 \pm 0.0096$ pb	$\sigma = 0.186 + 0.11 - 0.058$ pb (Sherpa (NLO QCD+ NLO EW corr))	JHEP 06 (2023) 080
Z [njet ≥ 3]	7	4.6	$\sigma = 3.09 \pm 0.03 \pm 0.4$ pb	$\sigma = 3.1 \pm 0.14$ pb (Blackhat)	JHEP 07, 032 (2013)
Z [njet = 2]	13	139	$\sigma = 1.941 \pm 0.004 \pm 0.061$ pb	$\sigma = 1.807 + 0.69 - 0.39$ pb (Sherpa (NLO QCD+ NLO EW corr))	JHEP 06 (2023) 080
Z [njet ≥ 2]	7	4.6	$\sigma = 15.05 \pm 0.06 \pm 1.51$ pb	$\sigma = 14.9 \pm 0.4$ pb (Blackhat)	JHEP 07, 032 (2013)
Z [njet = 1]	13	139	$\sigma = 11.74 \pm 0.01 \pm 0.33$ pb	$\sigma = 11.17 + 2.2 - 1.3$ pb (Sherpa (NLO QCD+ NLO EW corr))	JHEP 06 (2023) 080
Z [njet ≥ 1]	7	4.6	$\sigma = 68.84 \pm 0.13 \pm 5.15$ pb	$\sigma = 64.8 \pm 3.1$ pb (Blackhat)	JHEP 07, 032 (2013)
Z	13.6	1.2	$\sigma = 61.65 \pm 0.059 \pm 2.91$ nb	$\sigma = 64.83 + 1.25 - 1.34$ nb (NNLO(QCD)+NLO(EW))	ATLAS-CONF-2022-070
Z	13	3.2	$\sigma = 58.43 \pm 0.03 \pm 1.66$ nb	$\sigma = 55.96 + 1.5 - 1.7$ nb (DYNNLO+CT14 NNLO)	JHEP 02 (2017) 117
Z	8	20.2	$\sigma = 34.24 \pm 0.03 \pm 0.92$ nb	$\sigma = 32.94 + 0.8 - 0.92$ nb (DYNNLO+CT14 NNLO)	JHEP 02 (2017) 117
Z	7	4.6	$\sigma = 29.53 \pm 0.03 \pm 0.77$ nb	$\sigma = 28.31 + 0.68 - 0.8$ nb (DYNNLO+CT14 NNLO)	JHEP 02 (2017) 117

Figure 23: Measured cross-sections and associated predictions for the Bosons results displayed in all figures.

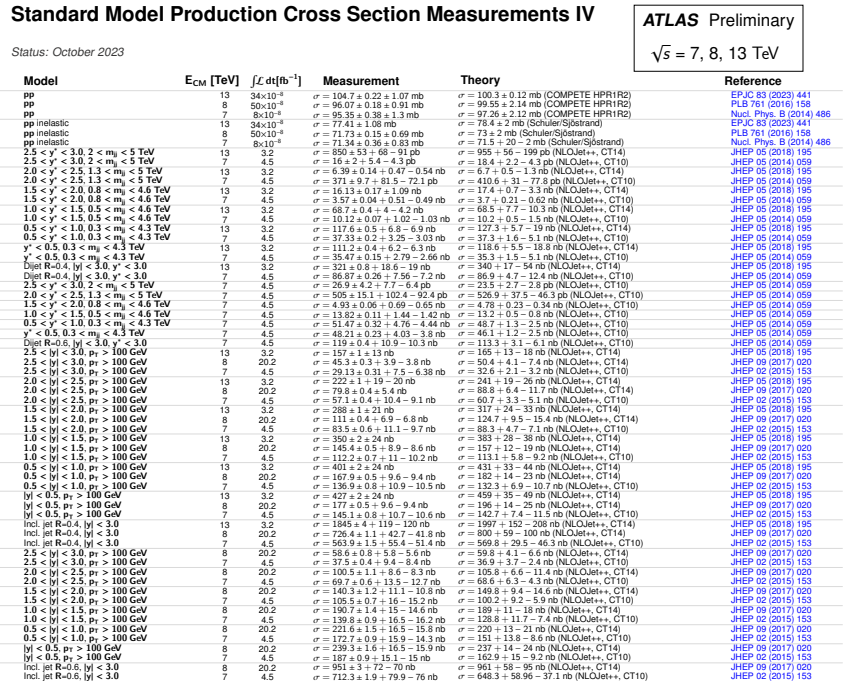

Figure 24: Measured cross-sections and associated predictions for the Jets results displayed in all figures.

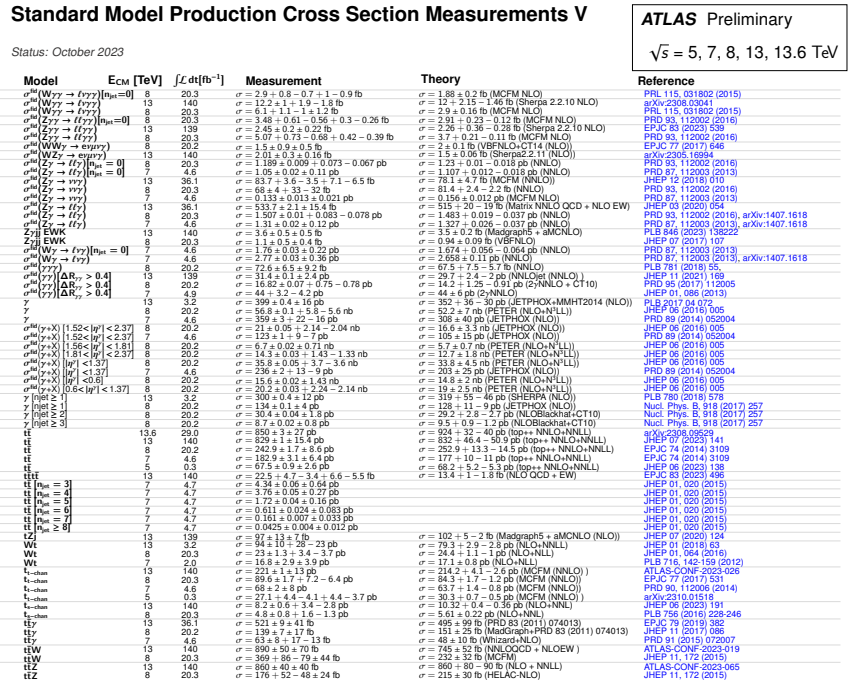

Figure 25: Measured cross-sections and associated predictions for the Photons and Top results displayed in all figures.

10 Cross-section measurements as a function of centre-of-mass energy $\sqrt{s}$

Summary of total production cross-section measurements by ATLAS presented as a function of centre-of-mass energy from 7 to 13 TeV for a few selected processes. The diboson measurements are scaled by a factor 0.1 to allow a presentation without overlaps.

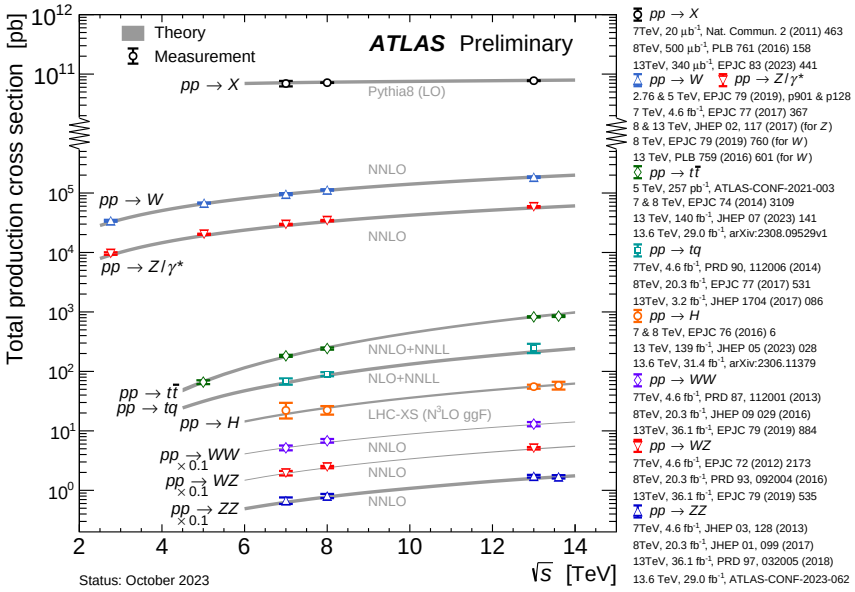

Figure 26: Summary of total production cross-section measurements by ATLAS presented as a function of centre-of-mass energy from 2.76 to 13.6 TeV for a few selected processes.

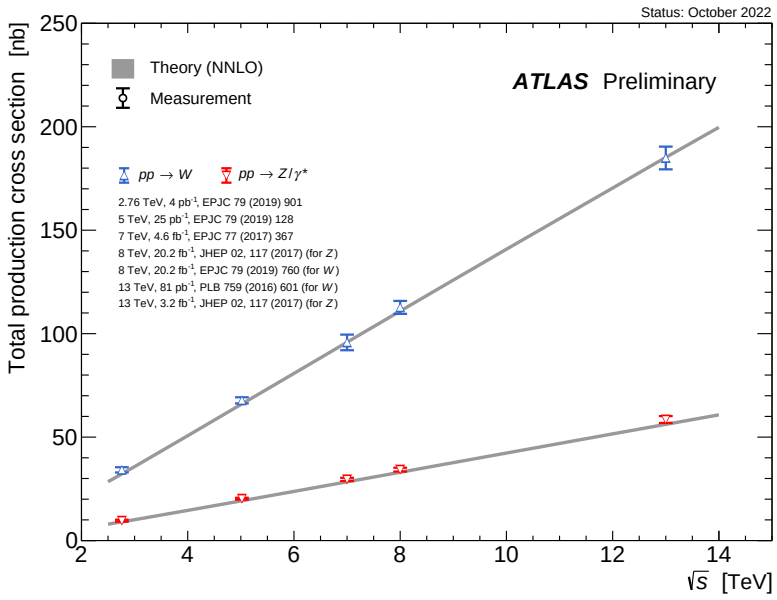

Figure 27: Summary of total production cross-section measurements of electro-weak gauge boson by ATLAS presented as a function of centre-of-mass energy from 2.76 to 13.6 TeV.

References

[1] ATLAS Collaboration, *Gitlab page for Summary plots*, (2020), URL: https://gitlab.cern.ch/atlas-physics/sm/StandardModelTools_SummaryPlots/SummaryPlots (cit. on p. 2).

[2] ATLAS Collaboration, *Standard Model Summary Plots February 2022*, (2022), URL: https://atlas.web.cern.ch/Atlas/GROUPS/PHYSICS/PUBNOTES/ATL-PHYS-PUB-2022-009/ (cit. on p. 2).

[3] ATLAS Collaboration, *Measurement of the total cross section and ρ-parameter from elastic scattering in pp collisions at $\sqrt{s}$ = 13 TeV with the ATLAS detector*, EPJC **83** (2022) 441 (cit. on p. 2).

[4] ATLAS Collaboration, *Observation of four-top-quark production in the multilepton final state with the ATLAS makedetector*, EPJC **83** (2023) 496 (cit. on p. 2).

[5] ATLAS Collaboration, *Measurement of single top-quark production in the s-channel in proton–proton collisions at $\sqrt{s}$ = 13 TeV with the ATLAS detector*, JHEP **06** (2023) 191 (cit. on p. 2).

[6] ATLAS Collaboration, *Measurements of Higgs bosons decaying to bottom quarks from vector boson fusion production with the ATLAS experiment at $\sqrt{s}$ = 13 TeV*, Eur. Phys. J. C **81** (2021) 537, arXiv: 2011.08280 [hep-ex] (cit. on p. 2).

[7] ATLAS Collaboration, *Measurement of t-channel single-top-quark production in pp collisions at $\sqrt{s}$ = 5.02 TeV with the ATLAS detector*, (2023), arXiv: 2310.01518 [hep-ex] (cit. on p. 2).

[8] *Measurement of t-channel production of single top quarks and antiquarks in pp collisions at 13 TeV using the full ATLAS Run 2 dataset*, (2023) (cit. on p. 2).

[9] *Measurement of the production cross-section in pp collisions at = 5.02 TeV with the ATLAS detector*, JHEP **06** (2023) 138 (cit. on p. 2).

[10] *Inclusive and differential cross-sections for dilepton $t\bar{t}$ production measured in $\sqrt{s}$ =13 TeV pp collisions with the ATLAS detector*, JHEP **07** (2023) 141 (cit. on p. 2).

[11] ATLAS Collaboration, *Measurement of the total and differential cross-sections of $t\bar{t}W$ production in pp collisions at $\sqrt{s}$ =13 TeV with the ATLAS detector*, tech. rep. ATLAS-CONF-2023-019, CERN, 2023, URL: https://atlas.web.cern.ch/Atlas/GROUPS/PHYSICS/CONFNOTES/ATLAS-CONF-2023-019 (cit. on p. 2).

[12] ATLAS Collaboration, *Inclusive and differential cross section measurements of $t\bar{t}Z$ production in pp collisions at $\sqrt{s}$ =13 TeV with the ATLAS detector, including EFT and spin correlations interpretations*, tech. rep. ATLAS-CONF-2023-065, CERN, 2023, URL: https://atlas.web.cern.ch/Atlas/GROUPS/PHYSICS/CONFNOTES/ATLAS-CONF-2023-065 (cit. on p. 3).

[13] ATLAS Collaboration, *Measurement of $Z\gamma\gamma$ production in pp collisions at $\sqrt{s}$ = 13 TeV with the ATLAS detector*, Eur. Phys. J. C **83** (2023) 539, arXiv: 2211.14171 [hep-ex] (cit. on p. 3).

[14] ATLAS Collaboration, *Observation of $W\gamma\gamma$ triboson production in proton-proton collisions at $\sqrt{s}$ = 13 TeV with the ATLAS detector*, (2023), arXiv: 2308.03041 [hep-ex] (cit. on p. 3).

[15] ATLAS Collaboration,
Observation of $WZ\gamma$ production in pp collisions at $\sqrt{s}$ = 13 TeV with the ATLAS detector, (2023), arXiv: 2305.16994 [hep-ex] (cit. on p. 3).

[16] ATLAS Collaboration, *Measurement and interpretation of same-sign W boson pair production in association with two jets in pp collisions at $\sqrt{s}$ = 13 TeV with the ATLAS detector*, tech. rep., 2023, URL: https://cds.cern.ch/record/2872564 (cit. on p. 3).

[17] ATLAS Collaboration, *Measurement of the $t\bar{t}$ cross-section and $t\bar{t}/Z$ cross-section ratio using LHC Run 3 pp collision data at a centre-of-mass energy of $\sqrt{s}$ = 13.6 TeV*,
tech. rep. ATLAS-CONF-2022-070, CERN, 2022, URL: https://atlas.web.cern.ch/Atlas/GROUPS/PHYSICS/CONFNOTES/ATLAS-CONF-2022-070/ (cit. on p. 3).

[18] ATLAS Collaboration, *Measurement of ZZ production cross-sections in the four-lepton final state in pp collisions at $\sqrt{s}$ =13 TeV with the ATLAS experiment*, tech. rep. ATLAS-CONF-2023-062, CERN, 2023, URL: https://atlas.web.cern.ch/Atlas/GROUPS/PHYSICS/CONFNOTES/ATLAS-CONF-2023-062/ (cit. on p. 3).

[19] ATLAS Collaboration, *Measurement of the $H \to \gamma\gamma$ and $H \to ZZ^* \to 4\ell$ cross-sections in pp collisions at $\sqrt{s}$ = 13.6 TeV with the ATLAS detector*, (2023), arXiv: 2306.11379 [hep-ex] (cit. on p. 3).

[20] ATLAS Collaboration, *Measurement of the $t\bar{t}$ cross section and its ratio to the Z production cross section using pp collisions at $\sqrt{s}$ = 13.6 TeV with the ATLAS detector*, (2023),
arXiv: 2308.09529 [hep-ex] (cit. on p. 3).